Available online at www.sciencedirect.com

ScienceDirect

Journal of Nutritional Biochemistry 113 (2023) 109247

Journal of Nutritional Biochemistry

RESEARCH PAPER

Skeletal muscle insulin resistance and adipose tissue hypertrophy persist beyond the reshaping of gut microbiota in young rats fed a fructose-rich diet

Arianna Mazzoli[a], Angela Di Porzio[a], Cristina Gatto[a], Raffaella Crescenzo[a,f], Martina Nazzaro[a], Maria Stefania Spagnuolo[b], Loredana Baccigalupi[c,f], Ezio Ricca[a,f], Angela Amoresano[d], Carolina Fontanarosa[d], Caterina Bernacchioni[e], Chiara Donati[e], Susanna Iossa[a,f,*], Luisa Cigliano[a,f]

[a] Department of Biology, University of Naples Federico II, Naples, Italy
[b] Department of Bio-Agrofood Science, Institute for the Animal Production System in Mediterranean Environment, National Research Council Naples (CNR-ISPAAM), Naples, Italy
[c] Department of Molecular Medicine and Medical Biotechnology, University of Naples Federico II, Naples, Italy
[d] Department of Chemical Sciences, University of Naples Federico II, Naples, Italy
[e] Department of Biomedical, Experimental and Clinical Sciences, University of Florence, Florence, Italy
[f] Task Force on Microbiome Studies, University of Naples Federico II, Naples, Italy

Received 13 May 2022; received in revised form 17 October 2022; accepted 2 December 2022

Abstract

To investigate whether short term fructose-rich diet induces changes in the gut microbiota as well as in skeletal muscle and adipose tissue physiology and verify whether they persist even after fructose withdrawal, young rats of 30 d of age were fed for 3 weeks a fructose-rich or control diet. At the end of the 3-weeks period, half of the rats from each group were maintained for further 3 weeks on a control diet. Metagenomic analysis of gut microbiota and short chain fatty acids levels (faeces and plasma) were investigated. Insulin response was evaluated at the whole-body level and both in skeletal muscle and epididymal adipose tissue, together with skeletal muscle mitochondrial function, oxidative stress, and lipid composition. In parallel, morphology and physiological status of epididymal adipose tissue was also evaluated. Reshaping of gut microbiota and increased content of short chain fatty acids was elicited by the fructose diet and abolished by switching back to control diet. On the other hand, most metabolic changes elicited by fructose-rich diet in skeletal muscle and epididymal adipose tissue persisted after switching to control diet. Increased dietary fructose intake even on a short-time basis elicits persistent changes in the physiology of metabolically relevant tissues, such as adipose tissue and skeletal muscle, through mechanisms that go well beyond the reshaping of gut microbiota. This picture delineates a harmful situation, in particular for the young populations, posed at risk of metabolic modifications that may persist in their adulthood.

Keywords: Fructose; Gut microbiota; Insulin resistance; Short chain fatty acids; Adipocyte; Skeletal muscle; Young.

1. Introduction

Increasing experimental evidence from both epidemiological and experimental investigations indicates that the elevated consumption of fructose-rich food and drinks contributes to the onset of insulin resistance and metabolic syndrome [1,2]. This occurs in all age groups, but the most alarming situation is that of young people. In fact, the HELENA study has evidenced that European adolescents consume about 1000 mL/d (corresponding to more than 1000 kJ/d) of beverages and fruit juices, containing fructose or high-fructose corn syrup as sweetener [3].

Although skeletal muscle is the primary site of whole-body glucose disposal [4] being therefore deeply involved in the establishment of insulin resistance [4], it has not been considered a primary tissue involved in the oxidation of fructose. Interestingly, it has been recently evaluated that about 15% of ingested fructose escapes splanchnic extraction and circulates in the periphery [5]. This result suggests that, besides liver and gut, other metabolically relevant tissues, such as skeletal muscle and white adipose tissue, could directly metabolize blood fructose, since they express the glucose transporter (GLUT)5 [6], and the enzyme fructokinase A [7]. Accordingly, Jang et al. [8], by using labelled fructose, evidenced utilization of this sugar in skeletal muscle and adipose tissue.

Several papers reported the deleterious effects of increased dietary intake of this sugar on skeletal muscle physiology. In particular, different lines of evidence showed insulin resistance development in skeletal muscle after fructose intake [9–13]. We also previ-

* Corresponding author at: Susanna Iossa, Department of Biology, Complesso Universitario Monte S.Angelo, Edificio 7, Via Cintia - I-80126 Napoli, Italy. Tel.:+39-081-2538111; fax: +39-081-679233.
E-mail address: susiossa@unina.it (S. Iossa).

https://doi.org/10.1016/j.jnutbio.2022.109247
0955-2863/

ously showed that adult rats develop insulin resistance in skeletal muscle, coupled with increased ceramide content, both after short [14] or long [15] term fructose intake.

It is now well documented that the development of cellular insulin resistance in skeletal muscle is strictly linked to mitochondrial dysfunction and oxidative stress [16]. Jaiswal et al. [17] demonstrated the onset of oxidative stress, mitochondrial dysfunction, and apoptosis in L6 myotubes exposed to fructose. De Stefanis et al. [18] confirmed the induction of apoptosis *in vivo* in mice after very long term fructose intake, while Warren et al. [19] found impaired mitochondrial function in glycolytic muscle after 6 weeks of 10% fructose solution administration. In addition, 7 d old rats receiving high fructose solution (20% w/v) for only 7 d exhibited decreased activity of catalase, depleted GSH and increased lipid peroxidation in skeletal muscle [20].

Similarly to the skeletal muscle, metabolic impairment was also evidenced in white adipose tissue (WAT), another tissue highly involved in glucose metabolism, with development of hypertrophy, inflammation and insulin resistance following increased fructose intake [21,22], even after only 4 weeks of dietary treatment [23].

Over the last decade, gut microbial modifications (composition and/or function) have been associated with aging, obesity, sugar-associated metabolic disorders, and insulin resistance [24,25]. Interestingly, while many studies investigated how the gut microbiota influences the liver and intestinal metabolism, immunity, and behavior [26–29], the importance of the gut microbiota for the control of energy homeostasis in adipose tissue and skeletal muscle has only recently emerged [30,31].

Another still unknown issue, related to elevated fructose consumption, is whether the metabolic derangement elicited by fructose-rich diet can be switched back when a healthy diet is reintroduced, or if it takes a long time to be corrected. This information is however of outmost importance to better delineate the harmful effects of this sugar, especially in the young population, which is at a critical time for the growth of muscle mass. To date, it has been only reported that switching from a high fat to low fat diet is able to reverse the metabolic phenotype [32], while we recently showed that liver alterations induced by 3 weeks of fructose-rich diet are still present 3 weeks after fructose withdrawal [33].

We therefore investigated whether short term fructose-rich diet in young rats induces changes in the gut microbiota and impacts on both skeletal muscle and adipose tissue physiology. Also, we verified whether, 3 weeks after fructose withdrawal, the physiological status of these tissues and the gut microbiota composition has been recovered. Moreover, considering that human mean fructose consumption is about 10% of total energy, with 95th percentile reaching an intake that correspond to 26% of total energy intake [34], we chose to carry out experiments using a fructose dose quite similar to the human consumption in order to increase the significance and transferability of the results to human health.

2. Methods

2.1. Animals and treatments

The study was conducted according to the guidelines of the Declaration of Helsinki, approved by "Comitato Etico-Scientifico per la Sperimentazione Animale" of the University of Naples Federico II and authorized by Italian Health Minister (4448/2019-PR).

Male Wistar rats (Charles River, Italy), of 30 d of age were caged in a temperature-controlled room (23±1°C) with a 12-h light/dark cycle (06.30–18.30) and unrestricted access to food. Rats were divided in two groups (each composed of 16 rats) that were fed for 3 weeks a fructose-rich (30% of calories coming from fructose) (F) or control (C) diet (composition in supplementary Table 1). At the end of the 3-weeks period, half of the rats (8 rats) from each group (F and C) were euthanized, while the other half of the rats from each group (eight rats) were maintained for further 3 weeks on a control diet and defined CR (rats fed a control diet for the first 3 weeks) and FR (rats fed a fructose-rich diet for the first 3 weeks). During the whole experimental period, food intake was monitored. At the end of the experimental period, rats were anesthetized with sodium pentothal (40 mg kg-1 i.p.) and euthanized by decapitation, and epididymal white adipose tissue (eWAT) and hindleg skeletal muscles (gastrocnemius, soleus, posterior tibialis and quadriceps, all rapidly dissected, freed of excess fat and connective tissue) were frozen in liquid nitrogen and stored at -80°C for further analyses. A small sample of eWAT was collected and fixed in 4% buffered formaldehyde.

2.2. Glucose tolerance test and plasma triglycerides

The day before the euthanasia, rats were fasted (from 8 a.m.) and after 6 h the basal postabsorptive blood samples were collected from tail vein in EDTA-coated tubes for plasma separation. Then, glucose (2 g kg^{-1}) was injected intraperitoneally and blood samples were taken after 20, 40, 60, 90 and 120 min.

Blood samples from glucose tolerance test were centrifuged at 1400xg for 8 min at 4°C, plasma was collected and stored at −20°C for further determination of glucose and insulin. Plasma glucose concentration was measured by a colorimetric enzymatic method (GS Diagnostics SRL, Guidonia Montecelio, Rome, Italy). Plasma insulin concentration was measured by an ELISA kit (Mercodia AB, Uppsala, Sweden) in a single assay to avoid interassay variations. Skeletal muscle insulin sensitivity was calculated according to Abdul-Ghani et al. [35] as the rate of decline in plasma glucose concentration from peak to nadir divided by mean plasma insulin concentration. Plasma samples obtained at time 0 of glucose tolerance test were also used for the determination of plasma triglycerides using a commercial kit (SGM Italia, Rome, Italy).

2.3. Tissue metabolites

Homogenates from skeletal muscle and eWAT were prepared in 50 mM phosphate buffer, pH 7.0 (1:50 w/v) and used to assess tissue content of fructose and uric acid by commercial kits based on colorimetric enzymatic methods (Sigma Aldrich, St. Louis, MO, USA for fructose, GS Diagnostics SRL, Guidonia Montecelio, Rome, Italy for uric acid).

Skeletal muscle triglycerides were quantified by using a commercial kit (SGM Italia, Rome, Italy), while tissue glycogen was assessed by direct enzymatic procedure [36].

Skeletal muscle ceramide content was evaluated by enzyme-linked immunosorbent assay (ELISA) as reported previously [37].

2.4. Fatty acid synthase activity

The activity of fatty acid synthase (FAS) was measured in eWAT and skeletal muscle homogenates prepared in KCl 175 mM, Tris 10 mM, pH 7.5 (1:8 w/v) as previously described [22]. Briefly, samples were incubated in a buffer containing KH_2PO_4 0.1 M, pH 6.5, acetyl-CoA 60 μM, malonyl-CoA 90 μM and NADPH 300 μM. The change in absorbance at 340 nm was measured, and one unit of activity was defined as that degrading 1 μmol of NADPH per minute at 37°C.

2.5. Oxidative stress parameters

Homogenates from eWAT and skeletal muscle were prepared in 50 mM phosphate buffer, pH 7.0 (1:50 w/v) and used for the determination of oxidative stress markers.

Lipid peroxidation was determined according to Fernandes et al. [38], by measuring thiobarbituric acid reactive substrates (TBARS), using the thiobarbituric acid assay.

Nitro-tyrosine (N-Tyr) titration was carried out by ELISA in tissue homogenates using rabbit anti-N-Tyr IgG (Covalab, distributed by VinciBiochem, Vinci, Italy; 1:600 dilution in T-TBS containing 0.25% BSA), followed by 60 μL of GAR-HRP (1:3500 dilution; 1 h, 37°C), as previously described [39].

Superoxyde dismutase (SOD) activity was measured in a medium containing 50 mM KH_2PO_4 pH 7.8, 20 mM cytochrome c, 0.1 mM xanthine, and 0.01 units of xanthine oxidase. Determinations were carried out spectrophotometrically (550 nm) at 25°C, by monitoring the decrease in the reduction rate of cytochrome c by superoxide radicals, generated by the xanthine-xanthine oxidase system. One unit of SOD activity is defined as the concentration of enzyme that inhibits cytochrome c reduction by 50% in the presence of xanthine+xanthine oxidase [40].

Catalase activity was measured in tissue homogenates in 50 mM phosphate buffer, pH 7.0 containing 10 mM H_2O_2 and 0.25% Triton X-100. Determinations were carried out spectrophotometrically (240 nm) at 25°C, by monitoring the decrease in absorbance due to the decomposition of H_2O_2. The rate of H_2O_2 loss from solution was linear when the natural log of the absorbance was plotted against time, in accord with the usual first-order kinetics exhibited by catalase [41]. Linear regression analysis was carried out to calculate the first order reaction rate constant (k) and the values were then referred to unit of tissue weight.

Glutathione reductase (GR) activity was measured by monitoring the decrease of NADPH absorbance at 340 nm at 30°C. The reaction mixture contained 0.2 M

potassium phosphate buffer, 2 mM EDTA, 2 mM NADPH (in 10 mM Tris-HCl, pH 7), and 20 mM oxidized glutathione. The activity was calculated using the NADPH molar extinction coefficient, 6.22×10^{-5}, considering that one unit of GR is defined the amount of enzyme that catalyzes the reduction of 1 μmol of NADPH per minute. The specific activity is expressed in mU per g of tissue.

Xanthine oxidase activity was measured in 50 mM KH_2PO_4, pH 7.5, containing 0.1 mM EDTA and 50 mM xanthine. Determinations were carried out spectrophotometrically (290 nm) at 37°C, by monitoring the increase in the absorbance due to the production of uric acid [42]. One unit of xanthine oxidase is defined as the amount of the enzyme that converts 1 μmol of xanthine into uric acid per minute.

NADPH oxidase activity was assayed according to a modification of the method of Bettaieb et al. [43]. Briefly, tissues (1:10 w/v) were homogenized in ice-cold Krebs buffer and then centrifuged at 800xg, at 4°C for 10 min. The supernatant was collected and then centrifuged at 30,000xg for 2 h at 4°C. The pellet (membrane fraction) was resuspended in Krebs buffer and protein concentration measured. Aliquots containing 100 μg of protein were added to Krebs buffer containing NADPH (500 μM). The change in absorbance at 340 nm was followed for 10 min at 30 s intervals.

2.6. Mitochondrial marker enzymes in skeletal muscle

Cytochrome oxidase (COX) activity was measured in skeletal muscles samples homogenized in a KCl medium containing, 100 mM KCl, 50 mM Hepes, 5 mM MgCl2, 1 mM EDTA, 5 mM EGTA, 1 mM ATP pH 7.0. Aliquots of homogenates were then incubated for 30 min at 0°C after the addition of 1.5 mg/mL lubrol.

Samples of tissue homogenates were transferred into calibrated Oxygraph-2 k (O2k, OROBOROS INSTRUMENTS, Innsbruck, Austria) 2 ml-chambers. Measurement of COX activity was carried out at 37°C in a medium containing 75 mM Hepes, 30 μM cytochrome c, 10 mM malonate, 4 μM rotenone, 0.5 mM dinitrophenol, 4 mM ascorbate and 0.3 mM N,N,N',N'-tetramethyl-P-phenylenediamine [44].

Citrate synthase (CS) activity was measured according to Srere [45]. Briefly, skeletal muscles were homogenized in a medium containing 1 M Tris, 1mM DTNB, 10 mM Acetyl-CoA, 10 mM Oxaloacetate, 0.5% Triton, pH 8.1. The appearance of the free SH group of the released CoASH was followed at 412 nm for 3 min at 30 s intervals, at 30°C. The results were expressed as μmolCoA/min x grams of tissue.

2.7. Inflammatory markers

Proteins were extracted from skeletal muscle and eWAT by homogenizing frozen tissues (-80°C) in ten volumes (w/v) of lysis buffer containing 20 mM Tris-HCl (pH 8), 138 mM NaCl, 2.7 mM KCl, 5% (v/v) glycerol, 1% (v/v) Nonidet P-40, 5 mM EDTA and 50 μL/g tissue of protease inhibitor cocktail and 10 μL/g of phosphatase inhibitor cocktail (all from Sigma-Aldrich, St. Louis, MO, USA). Homogenates were centrifuged at 12000xg for 10 min at 4°C and the supernatants were collected and used for the determination of tumor necrosis factor α (TNF-α) concentrations, using a rat specific enzyme linked immunosorbent assay (ELISA) (R&D Systems, Minneapolis, MN, USA) according to manufacturer's instruction.

Myeloperoxidase (MPO) activity was assessed as previously described [46] on eWAT samples (100 mg) that were homogenized in 1 mL of hexadecyltrimethylammonium bromide (HTAB) buffer (0.5% HTAB in 50 mM phosphate buffer, pH 6.0).

2.8. Histopathological analysis of eWAT

Immunostaining was carried out essentially as described by Cinti et al. [47]. Briefly, after fixation in 4% buffered formaldehyde, eWAT was embedded in paraffin, and cut into 5 μm thick sections. Immunohistochemistry was performed on dewaxed 5 μm serial sections using 3% hydrogen peroxide to inactivate endogenous peroxidases followed by normal horse serum to reduce non-specific staining. Consecutive serial sections were incubated overnight (4°C) with antibodies for MAC-2/galectin-3 (1:200; Invitrogen, Carlsbad, CA, USA) and then incubated for 1 h at room temperature with biotinylated, horse anti-mouse IgG (MAC2/galectin-3) secondary antibody (Vector Laboratories, Burlingame, CA). Histochemical reactions were performed using the Vectastain ABC Kit (Vector Laboratories) and Sigma Fast 3,3 -diaminobenzidine as substrate (Sigma, St. Louis, MO). Sections were counterstained with hematoxylin. MAC2-positive crown like structure (CLS) per field were counted manually, and the percentage of CLSs per total number of nuclei per field was used as a measure of adipose tissue macrophage content. Images were acquired at a 20× magnification.

Adipocytes size distributions analysis was performed by computer image analysis of tissue sections according to Chen et al. [48].

2.9. Western blot analysis

Proteins were extracted from skeletal muscle and eWAT by homogenizing frozen tissues (-80°C) in ten volumes (w/v) of lysis buffer containing 20 mM Tris-HCl (pH 8), 138 mM NaCl, 2.7 mM KCl, 5% (v/v) glycerol, 1% (v/v) Nonidet P-40, 5 mM EDTA and 50 μL/g tissue of protease inhibitor cocktail and 10 μL/g tissue of phosphatase inhibitor cocktail (all from Sigma-Aldrich, St. Louis, MO, USA). Homogenates were centrifuged at 12000xg for 10 min at 4°C and the supernatants were collected. Aliquots of protein extracts were denatured in a buffer (60.0 mmol/l Tris, pH 6.8, 10% sucrose, 2% SDS, 4% β-mercaptoethanol) and loaded on a 12% sodium dodecyl sulphate (SDS)–polyacrylamide gel. After the run in electrode buffer (50 mmol/l Tris, pH 8.3, 384 mmol/l glycine, 0.1% SDS), the gels were transferred on PVDF membranes at 0.8 mA/cm^2 for 90 min. The membranes were preblocked in blocking buffer (PBS, 3% bovine albumin serum, 0,3% Tween 20) for 1 h and then incubated overnight at 4°C with antibodies for p-Akt (Cell Signaling, Danvers, MA, USA, code n. 4060; diluted 1:1000 in blocking buffer), p-glycogen synthase kinase (GSK) (Santa Cruz Biotechnology, Santa Cruz, CA, USA; 200μg/ml in blocking buffer), peroxisome proliferator-activated receptor alpha (PPAR-α) (Thermo Fisher, IL, USA, code n. PA1-32484; 0,5 mg/mL in blocking buffer), peroxisome proliferator-activated receptor gamma (PPAR-γ) (Santa Cruz Biotechnology, Santa Cruz, CA, USA; diluted 1:200 in blocking buffer), peroxisome proliferator-activated receptor gamma coactivator 1-alpha (PGC-1α) (Millipore, Billerica, MA, USA; 1:1000 in blocking buffer), GLUT5 (Invitrogen, Carlsbad, CA, USA, 0.5 μg/mL in blocking buffer), GLUT4 (Santa Cruz Biotechnology, Santa Cruz, CA, USA; diluted 1:200 in blocking buffer), adiponectin (Immunological Sciences, Rome, Italy, 1:1000 in blocking buffer), sphingosine kinase (SK1, SK2) (ECM Biosciences, Versailles, KY, USA, 1:1000 in blocking buffer), spinster homolog 2 (Spns2) (Merck Life Science, Burlington, MA, USA, 1:1000 in blocking buffer), sphingosine 1-phosphate ($S1P_1$, $S1P_3$) (Bioss Antibodies Inc, Woburn, MA, USA, 1:1000 in blocking buffer), $S1P_2$ (Proteintech, Rosemont, IL, USA, 1:1000 in blocking buffer). Membranes were washed three times for 7 min in PBS/0.3% Tween 20, and then incubated for 1 h at room temperature with an anti-rabbit, HRP-conjugated secondary antibody. The membranes were washed as described above, rinsed in distilled water, and incubated at room temperature with a chemiluminescent substrate, Immobilon HRP substrate (Millipore Corporation, Billerica, MA 01821, USA). Quantitative densitometry of the bands was carried out by analyzing chemidoc or digital images of X-ray films exposed to immunostained membranes. Quantification of signals was carried out by Image Lab Software (Biorad). Akt was detected with monoclonal antibody (Cell Signaling, Danvers, MA, USA; diluted 1:1000 in blocking buffer), GSK was detected with monoclonal antibody (Santa Cruz Biotechnology, Santa Cruz, CA, USA; diluted 1:1000 in blocking buffer). After the detection of p-Akt or p-GSK, the membranes were stripped for 30 min at 50°C in a solution containing glycine 25 mM, SDS 1%, pH 2 and then processed for quantification of Akt or GSK levels. Actin was detected with polyclonal antibody (Sigma-Aldrich, St Louis, MO, USA; diluted 1:1000 in blocking buffer) and used to normalize the PPAR-α, PPAR-γ, PGC-1α, adiponectin, GLUT4 and GLUT5 signals. The data of each marker are normalized to controls.

2.10. Gut microbiota analysis

Faecal samples (500 mg) were collected from the four experimental groups at the end of all dietary treatments and total DNA was extracted using the QIAamp DNA Stool Mini Kit (QIAGEN) following the manufacturer's instructions.

Partial 16S rRNA gene sequences were amplified using primer pairs Probio_Uni and Probio_Rev, targeting the V3 region of the 16S rRNA gene [49]. Amplicon checks were carried out as previously described [49]. The 16S rRNA gene sequencing was performed using a MiSeq (Illumina) at the DNA sequencing facility of GenProbio srl (www.genprobio.com) according to the protocol previously reported [49].

After sequencing and demultiplexing, the obtained reads of each sample were filtered to remove low quality and polyclonal sequences. All quality-approved, trimmed and filtered data were exported as .fastq files that were processed using a script based on the QIIME software suite [50]. Paired-end reads pairs were assembled to reconstruct the complete Probio_Uni/Probio_Rev amplicons. Following a quality control, sequences with a length between 140 and 400 bp and mean sequence quality score >20 were retained. Sequences with homopolymers >7 bp and mismatched primers were omitted.

In order to calculate downstream diversity measures (alpha and beta diversity indices, UniFrac analysis), 16S rRNA Operational Taxonomic Units (OTUs) were defined at ≥ 100% sequence homology using DADA2 [51] and OTUs not encompassing at least two sequences of the same sample were removed. All reads were classified to the lowest possible taxonomic rank using QIIME2 [50,52] and the SILVA database v. 132 as reference dataset [53]. Biodiversity of the samples (alpha-diversity) was calculated with Chao1 and Shannon indexes. Similarities between samples (beta-diversity) were calculated by weighted UniFrac [54]. The range of similarities is calculated between the values 0 and 1. PCoA representations of beta-diversity were performed using QIIME2 [50,52]. Differential abundance testing at genus level was performed using the Analysis of Composition of Microbiomes (ANCOM-II) method [55] selecting a cut-off at 0.7.

2.11. Faecal and serum SCFAs extraction and derivatization

For short chain fatty acids (SCFAs) extraction, 100 mg of faecal samples and 100 μl of serum were used for the analysis. Faecal samples were grounded using liquid nitrogen. After, the samples were mixed with 9% formic acid, incubated with shaking for 2 h and then centrifugated at 10000 rpm for 15 min. The supernatant was extracted with ethyl acetate. For the derivatization 50 μl of BSTFA was added.

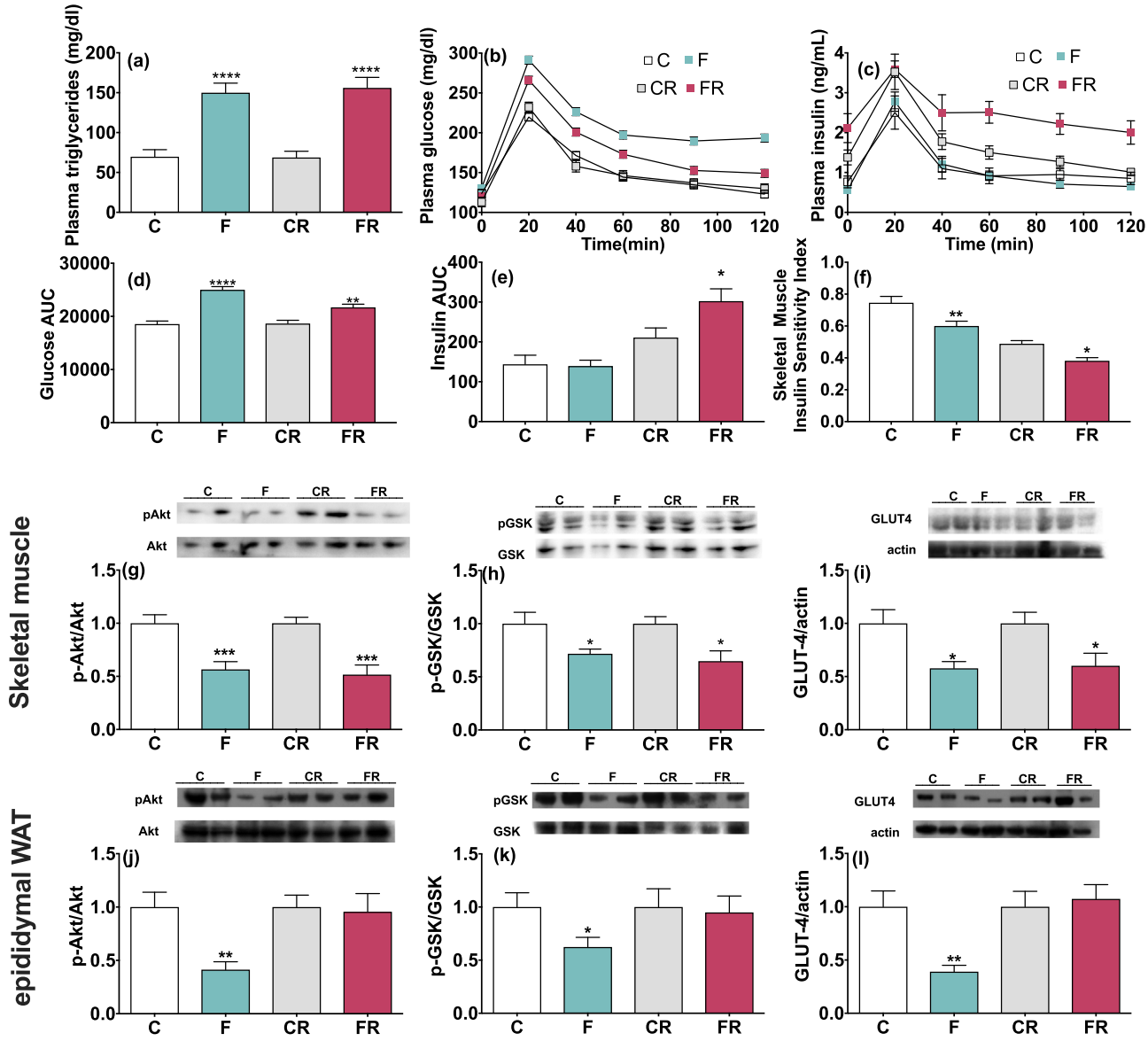

Fig. 1. Plasma levels of triglycerides (A), glucose (B), insulin (C), area under the curve (AUC) of glucose (D) and insulin (E), skeletal muscle insulin sensitivity index (F), Western blot quantification (with representative western blot) of phosphorylated kinase Akt (G, J), phosphorylated glycogen synthase kinase (GSK) (H, K), and glucose transporter 4 (GLUT4) (I, L) in skeletal muscle (G, H, I) and epididymal WAT (J, K, L) in control (C), fructose (F), control rescue (CR), and fructose rescue (FR) rats. Values are the means ± SEM of 8 different rats. $^{*}P<.05$, $^{**}P<.01$, $^{***}P<.001$, $^{****}P<.0001$ compared to respective controls (one-way ANOVA followed by Bonferroni post-test).

The reaction was conducted for 30 min at 90°C. Finally, the samples were dried, reconstituted in hexane and analyzed by GC/MS.

2.12. GC/MS analysis

GC/MS analysis was performed by a 7820A (Agilent Technologies, Santa Clara, CA, USA) with a HB-5 ms capillary column (30 m × 0.25 mm × 0.25 μm film thickness) (Agilent Technologies). The injector, ion source, quadrupole, and the GC/MS interface temperature were 230, 230, 150, and 280 °C, respectively. The flow rate of helium carrier gas was kept at 1 mL/min. 1 μl of derivatized sample was injected with a 3 min of solvent delay time and split ratio of 10:1. The initial column temperature was 40 °C and held 2 min, ramped to 150 °C at the rate of 15 °C/min and held 1 min, and then finally increased 280 °C at the rate of 30 °C/min and kept at this temperature for 5 min. The ionization was carried out in the electron impact (EI) mode at 70 eV.

The MS data were acquired in full scan mode from m/z 40–400 with acquisition frequency of 12.8 scans per second. The identification of compounds was confirmed by injection of pure standards and comparison of the retention time and corresponding EI MS spectra. The contents of SCFAs were calculated with external standard methods.

2.13. Statistical analysis

Data were expressed as mean values ± SEM. The program GraphPad Prism 6 (GraphPad Software, San Diego, CA, USA) was used to verify that raw data have normal distribution and to perform one-way ANOVA followed by Bonferroni post-test. A probability < 5% ($P<.05$) was considered statistically significant in all analyses.

3. Results

3.1. Metabolic parameters and insulin signaling

Fructose-rich diet, which is isocaloric compared to control diet (Table S1), had no effect on food intake during the experimental period. In fact, cumulative food intake in the 3-weeks period

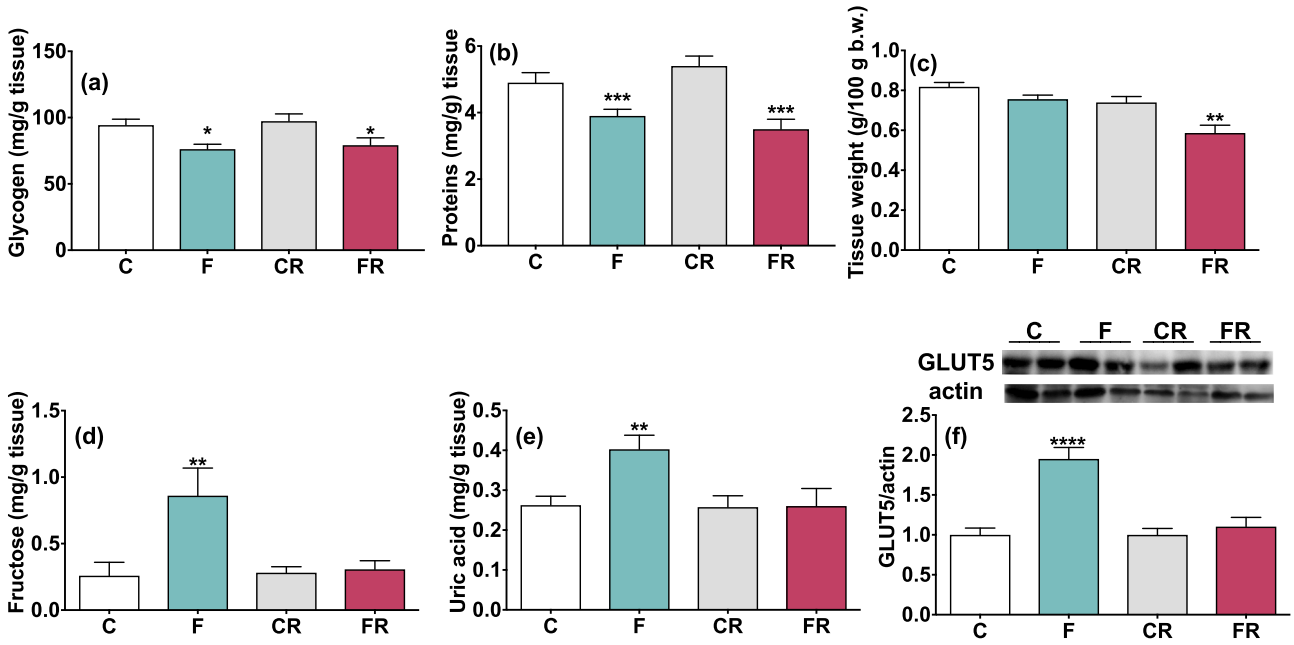

Fig. 2. Content of glycogen (A), and proteins (B), tissue weight (C), content of fructose (D), uric acid (E) and western blot quantification (with representative western blot) of glucose transporter 5 (GLUT5) (F) in skeletal muscle from control (C), fructose (F), control rescue (CR), and fructose rescue (FR) rats. Values are the means ± SEM of 8 different rats. *P<.05, **P<.01, ***P<.001, ****P<.0001 compared to respective controls (one-way ANOVA followed by Bonferroni post-test).

was 680±9 g for C rats (whose final body weight was 300±5 g) and 690± 10 g for F rats (whose final body weight was 303±5 g). Similarly, fructose-rich diet withdrawal had no effect on food intake, that was 700±8 g for CR rats (whose final body weight was 365±5 g) and 710±9 g for FR rats (whose final body weight was 380±5 g). Thus, all the metabolic effects found in F and FR rats could not be attributed to difference in energy intake between the groups.

The impact of dietary fructose on plasma triglycerides and on the regulation of systemic insulin sensitivity was investigated at the whole-body level. Plasma triglycerides were significantly increased in F rats in comparison to C rats and remained higher also in FR rats compared to CR rats (Fig. 1A).

Plasma glucose levels (Fig. 1B), quantified by calculating glucose area under the curve (AUC) during glucose tolerance test (Fig. 1D), were significantly higher in F rats compared to C rats, and remained higher in FR rats compared to CR rats. Plasma insulin levels (Fig. 1C), quantified by insulin AUC (Fig. 1E), were significantly higher in FR rats compared to CR rats. In addition, the skeletal muscle insulin sensitivity index was found to be significantly lower in F rats compared to C rats and in FR rats compared to CR rats (Fig. 1F).

To gain further insight into the mechanisms underlying insulin resistance, we assessed the degree of activation of two effectors of the insulin signaling pathway, namely Akt and GSK, both in skeletal muscle and eWAT. In skeletal muscle, the degree of activatory phosphorylation of Akt was significantly lower in F rats and remained decreased in FR rats compared to the respective controls (Fig. 1G). Accordingly, the degree of inhibitory phosphorylation of GSK was significantly lower in F rats and this decrease persisted in FR rats, compared to respective controls (Fig. 1H). In agreement with the lower activation of the intracellular signaling pathway of insulin, a lower protein content of the glucose transporter GLUT4 was found in F and FR rats, compared to their respective controls (Fig. 1I). In eWAT, the same three molecular markers of insulin signaling pathway were all lower in F rats but returned to control values in FR rats (Fig. 1J,K,L).

3.2. Skeletal muscle metabolites

Glycogen deposition in skeletal muscle, an indirect index of insulin action on this tissue, significantly decreased in F and FR rats, compared to their respective controls (Fig. 2A). In addition, a fructose-induced decrease in hindleg skeletal muscle protein content (Fig. 2B) was found in F and FR rats, compared to their respective controls, while tissue weight was significantly lower only in FR rats (Fig. 2C). Skeletal muscle content of fructose and its main metabolite, *i.e.,* uric acid, was significantly higher in F rats but returned to control levels in FR rats (Fig. 2D,E), in agreement with previous findings on plasma levels of the above metabolites measured in the same experimental paradigm [33]. The same pattern of regulation (*i.e.,* increased in F rats and reversed to control values in FR rats) was evident in the abundance of the fructose transporter GLUT5 (Fig. 2F).

Since fructose is a well-known positive regulator of de novo lipogenesis, we assessed the activity of the lipogenic enzyme FAS, that indeed was found increased in skeletal muscle from F and FR rats, compared to their respective controls (Fig. 3A). Accordingly, the content of triglycerides significantly increased in F rats and this increase persisted in FR rats (Fig. 3B). Similarly, the bioactive sphingolipid ceramide increased in F and FR rats (Fig. 3C). Ceramide can be deacylated to sphingosine that, in turn, can be phosphorylated to S1P by the enzyme SK1/SK2. Ceramide and S1P are interconvertible lipids, and it has been proposed that their relative intracellular levels dictate the cell fate evoking opposite biological effects [56]. Most of S1P biological actions are evoked, after its extracellular release through unspecific and specific (Spns2, spinster homolog 2) transporters, by its binding to G protein-coupled receptors named S1PR ($S1P_{1-5}$) in an autocrine/paracrine manner [57]. We therefore assessed the protein content of the two en-

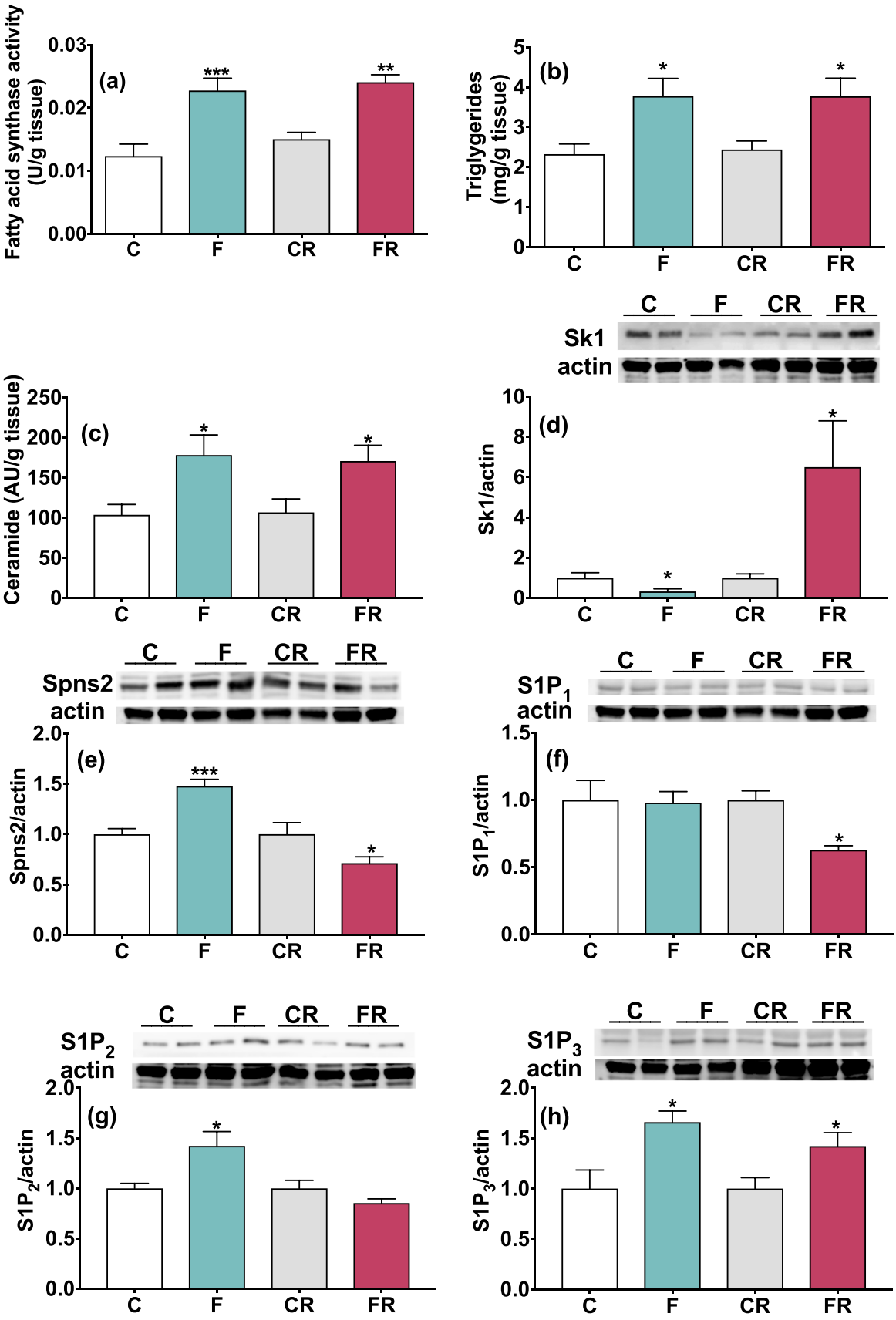

Fig. 3. Fatty acid synthase activity (A), quantification of triglycerides (B), ceramide (C), and western blot quantification (with representative western blot) of SK1 (D), Spns2 (E), S1P1 (F), S1P2 (G), S1P3 (H) in skeletal muscle from control (C), fructose (F), control rescue (CR), and fructose rescue (FR) rats. Values are the means ± SEM of 8 different rats. $^{*}P<.05$, $^{***}P<.001$ compared to respective controls (one-way ANOVA followed by Bonferroni post-test).

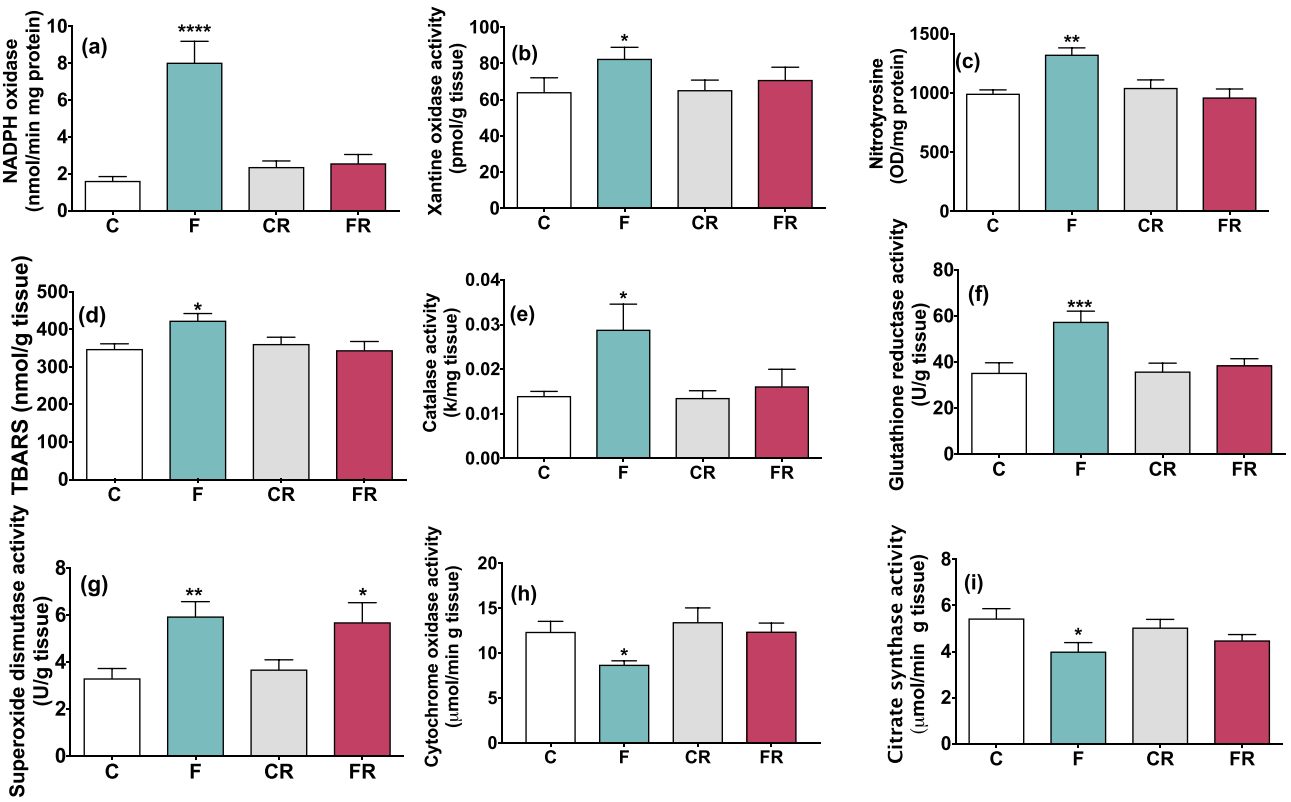

Fig. 4. Activity of NADPH oxidase (A) and xanthine oxidase (B), level of nitrotyrosine (N-Tyr) (C) and lipid peroxidation (D), activity of antioxidant enzymes catalase (E), glutathione reductase (F) and superoxide dismutase (G), activity of cytochrome oxidase (H) and citrate synthase (I) in skeletal muscle from control (C), fructose (F), control rescue (CR), and fructose rescue (FR) rats. Values are the means ± SEM of 8 different rats. *P<.05, ** P<.01, *** P<.001, **** P<.0001 compared to respective controls (one-way ANOVA followed by Bonferroni post-test).

zymes responsible for S1P synthesis, namely SK1 and SK2. SK1 was found significantly decreased in F rats, while being higher in FR rats (Fig. 3D), and no variation was evident in SK2 (data not shown). We also evidenced a fructose-induced increase in the specific S1P transporter Spns2 (Fig. 3E), as well as in the S1P receptors $S1P_2$ and $S1P_3$ (Fig. 3G,H). These latter variations were reversed by switching to control diet, except the increased $S1P_3$.

3.3. Oxidative status and mitochondrial function in skeletal muscle

Fructose-rich diet induced a significant increase in two important oxidant-producing enzymes, namely NADPH oxidase and xanthine oxidase (Fig. 4A,B). Accordingly, a condition of increased oxidative stress was detected both in the lipid and protein component of skeletal muscle (reflected in higher TBARS and N-Tyr levels) in F rats, that was reversed in FR rats (Fig. 4C,D). This increased oxidative stress was induced notwithstanding the compensative increase in the antioxidant enzymes catalase, GR and SOD (Fig. 4E,F,G). Almost all the above modifications, which were evident in F rats, switched back to control values in FR rats, except the increased SOD activity, that persisted in FR rats.

Skeletal muscle mitochondrial function has been repeatedly linked to the onset of insulin resistance. In addition, the mitochondria are one of the main cellular sites involved in the generation of ROS and hence in the induction of cellular oxidative stress. We therefore considered of interest to evaluate the putative mitochondrial changes elicited by high-fructose intake. To this end, we evaluated the activity of two mitochondrial marker enzymes, COX, located in the inner mitochondrial membrane, and CS, located in the mitochondrial matrix. Both enzymes decreased their activity in F rats, but returned to the control level in FR rats (Fig. 4H,I). The decrease found in mitochondrial enzymes is probably the result of regulation at the single enzyme level rather than changes in organelle mass/number, since no variation was found in the protein expression of three protein regulators of mitochondrial biogenesis, namely PGC-1α, PPARα and PPARγ (data not shown).

3.4. Epididymal white adipose tissue

eWAT is among the largest and most readily accessible fat pads in the rat [58] and its increase is associated with an increased risk for insulin resistance and dyslipidemia, since its surgical removal in rats and mice was shown to improve insulin action [59,60]. For these reasons, we choose to quantify eWAT mass changes after 3 or 6 weeks of dietary treatment (Fig. 5). This tissue exhibited an age-related increase during the first 3 weeks, with no difference between C and F rats (Fig. 5A). In the subsequent 3 weeks, eWAT gain, as well as tissue mass/unit body weight, was significantly higher in FR rats compared to CR rats (Fig. 5A,B). To assess the degree of hypertrophy of eWAT, we evaluated the distribution of cells with different diameter, and we found that the smaller adipocytes were significantly decreased after fructose-rich diet, while the larger adipocytes were significantly increased, compared to respective controls, so that the mean adipocyte area was significantly higher in F and FR rats compared to their respective controls (Fig. 5C,D). eWAT also exhibited an increase in fructose and uric acid content, coupled with an increased protein expres-

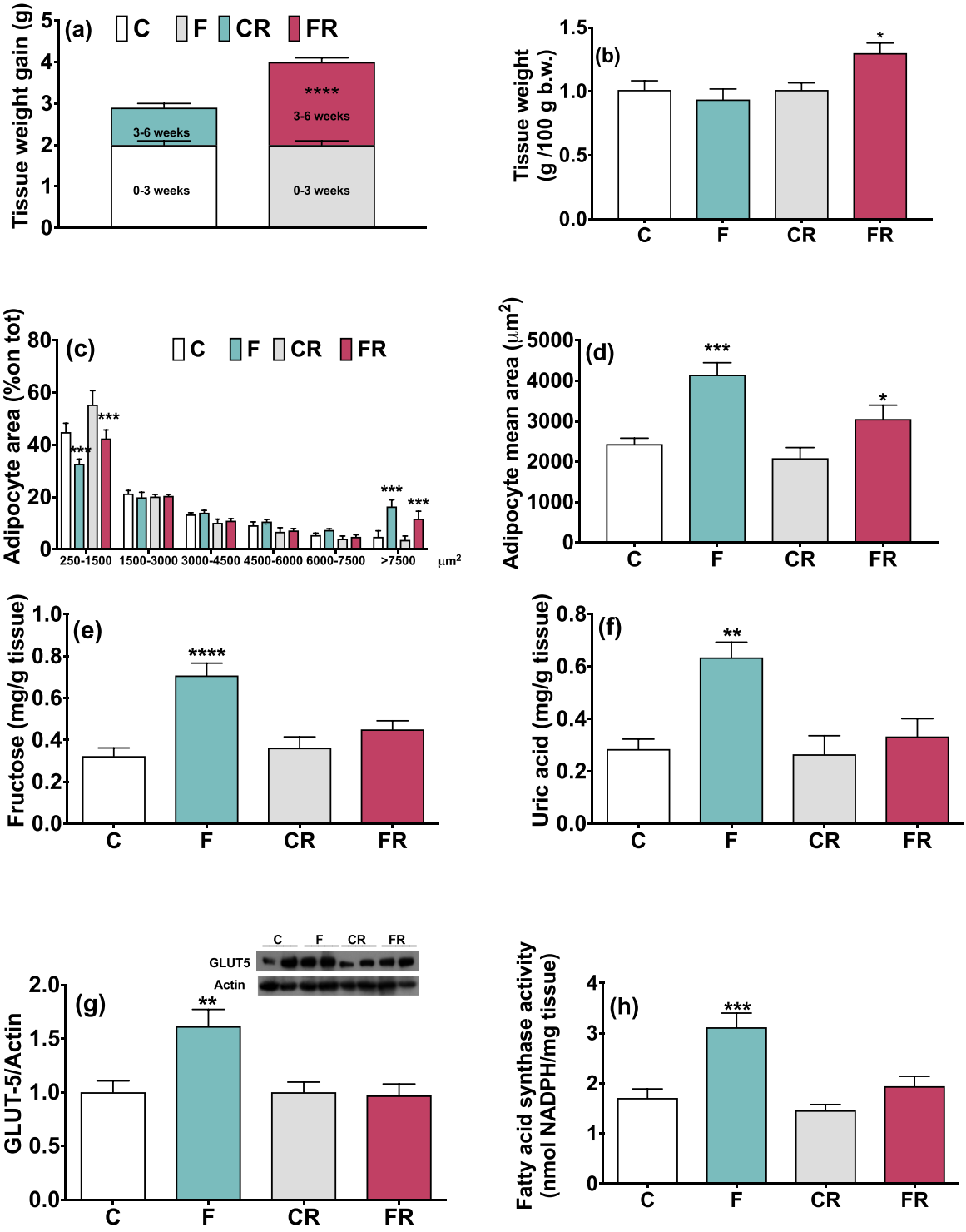

Fig. 5. Tissue weight gain (A), tissue weight (B), adipocyte area distribution (C) and mean adipocyte area (D), quantification of fructose (E), uric acid (F) western blot quantification (with representative western blot) of glucose transporter 5 (GLUT5) (G) and fatty acid synthase activity (H) in eWAT from control (C), fructose (F), control rescue (CR), and fructose rescue (FR) rats. Values are the means ± SEM of 8 different rats. *P<.05, ** P<.01, *** P<.001, ****P<.0001 compared to respective controls (one-way ANOVA followed by Bonferroni post-test).

sion of GLUT5 and increased FAS activity in F rats, and all these parameters went back to control values in FR rats (Fig. 5E,F,G,H). A condition of local inflammation of the tissue was also detected, as indicated by increased tissue content of TNF-α, increased MPO activity and increased presence of CLS, with a significant decrease in the anti-inflammatory mediator adiponectin (Fig. 6). All the above modifications found in eWAT persisted after switching to a control diet in FR rats. At variance with the above results, no sign of fructose-induced oxidative stress was detected in eWAT (data not shown).

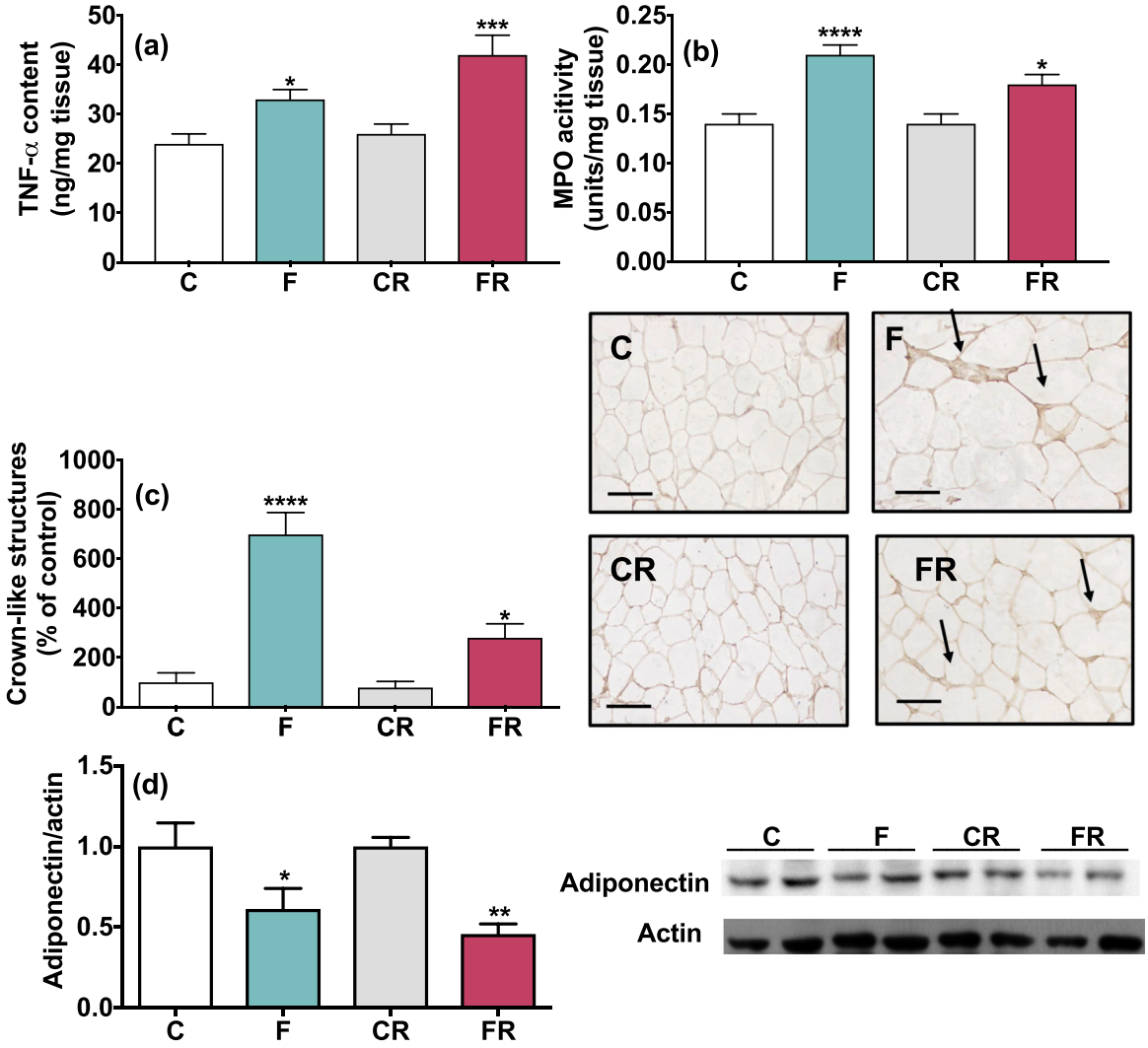

Fig. 6. TNF-α content (A), activity of myeloperoxidase (B), quantification of crown-like structure (CLS) (C), and western blot quantification (with representative blot) of adiponectin (D) in epididymal white adipose tissue from control (C), fructose (F), control rescue (CR), and fructose rescue (FR) rats. Values are the means ± SEM of 8 different rats. *P<.05, ** P<.01, ***P<.001, **** P<.0001 compared to respective controls (one-way ANOVA followed by Bonferroni post-test).

3.5. Gut microbiota and short chain fatty acids analysis

A 16S DNA-sequencing approach was used to investigate the effect of the various treatments on the gut microbial composition. The analysis of alpha diversity showed that F rats have increased diversity respect to C rats, as estimated by Shannon index (Fig. S1a) reflecting the diversity of OTUs in samples and Chao1 index (Fig.S1b), reflecting the OTUs abundance in the samples. No statistically significant difference of alpha diversity was observed between CR and FR groups, suggesting that the effect due to the fructose-rich diet was reversed by the reintroduction of a standard diet (Fig. S1).

A PCoA analysis based on Bray–Curtis distance (Fig. 7A) indicated that F rats clustered independently respect to the C rats, indicating that the fructose treatment, as expected, affected the bacterial composition of the gut. The same analysis also showed that animals treated with fructose for 3 weeks and then fed a control diet for the following 3 weeks (FR rats), clustered together with the respective controls (CR), consisting of animals treated with control diet for 6 weeks. This finding indicates that the gut microbiota is strongly influenced by the diet and that it is a very dynamic community that quickly responds to the diet changes.

To identify the bacterial genera specifically altered by diet we performed an ANCOM-II analysis selecting a cut-off of 0.7 [55]. Limiting the analysis to the bacterial genera with a relative abundance higher than 0.05%, 12 genera were found differently represented in the microbiota of the F group with respect to the control, showing that the high-fructose diet affected the gut microbial composition (Fig. 7B). In particular, we observed that 9 genera increased, and three genera decreased in the F group respect to the control. Comparing the FR group with the respective control (CR), no statistically significant differences were observed. These data indicate that a standard diet can completely restore the microbial changes induced by the fructose treatment.

The main SCFA of gut bacterial origin, namely acetate, propionate, and butyrate, were assessed in faeces and plasma (Fig. 8) by gas chromatography coupled to mass spectrometry. The faecal content of all the three SCFA significantly increased in F rats, while no variation was found in FR rats, compared to their respective controls (Fig. 8A,B,C). Plasma levels of propionate and butyrate were significantly higher in F rats, while acetate did not exhibit any fructose-induced variation (Fig. 8DD,E,F). After switching back to control diet, the concentrations of propionate and butyrate were restored to control levels.

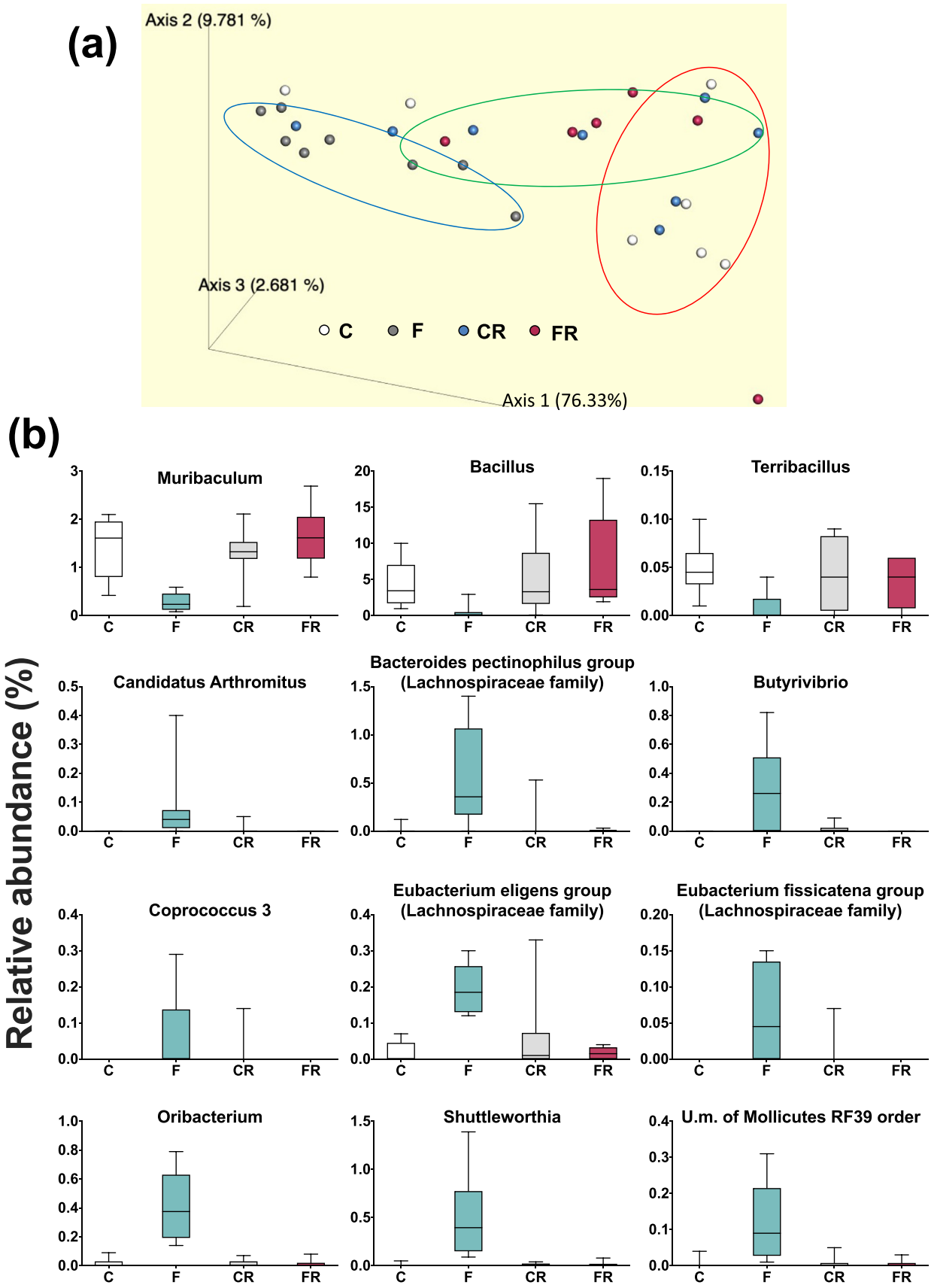

Fig. 7. Principal Coordinates Analysis (PCoA) (A) and analysis of composition of microbiome (ANCOM) on fecal microbiota at genus level (B) in control (C), fructose (F), control rescue (CR), and fructose rescue (FR) rats. Only genera showing differential abundance in F rats compared to C rats are shown as mean relative percentage abundance. Values are the means ± standard deviation of 8 different rats.

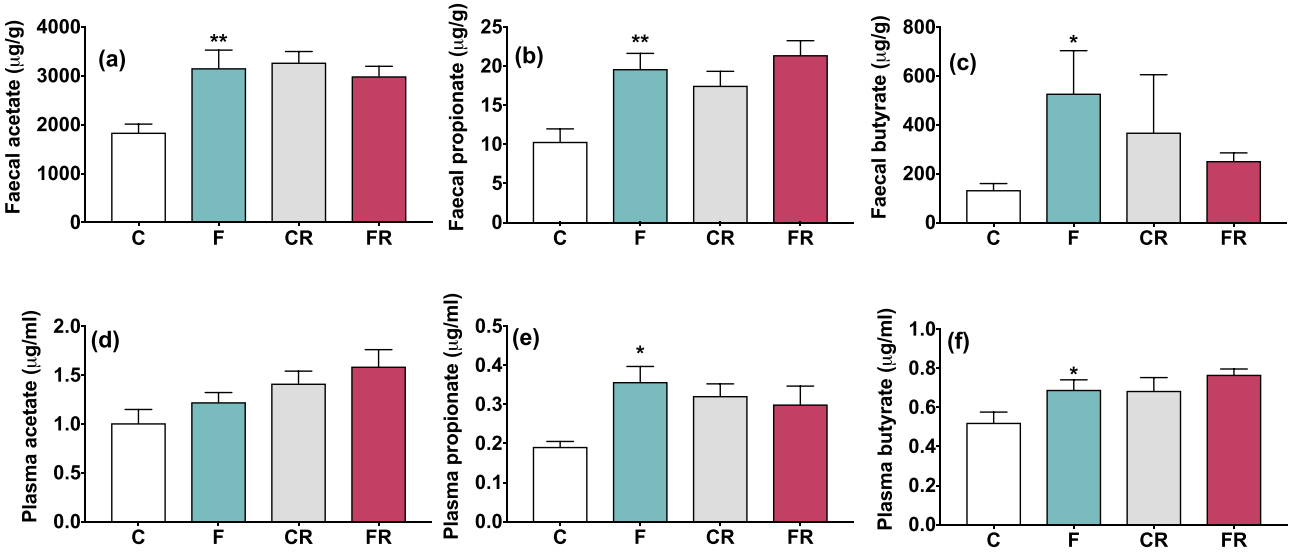

Fig. 8. Quantification of acetate, propionate and butyrate in faecal samples (A, B, C) and plasma samples (D, E, F) from control (C), fructose (F), control rescue (CR), and fructose rescue (FR) rats. Values are the means ± SEM of 8 different rats. $^{*}P<.05$, $^{**}P<.01$ compared to respective controls (one-way ANOVA followed by Bonferroni post-test).

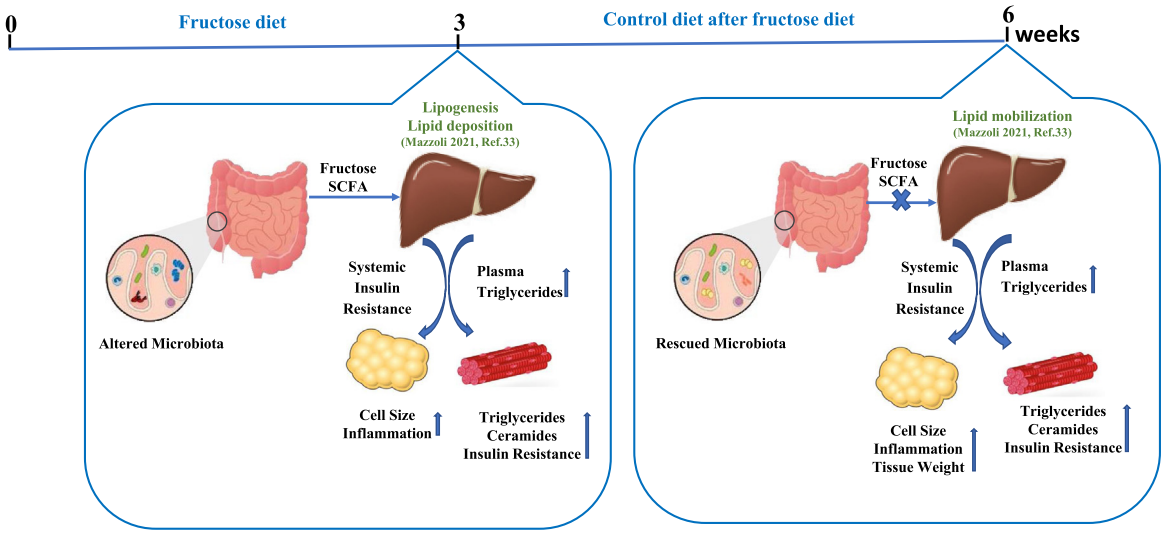

Fig. 9. Summary of changes in gut microbiota, skeletal muscle and epididymal white adipose tissue after short term fructose intake and their persistence after fructose removal from the diet.

4. Discussion

The hypothesis of a cross talk between gut microbiota, skeletal muscle and white adipose tissue has recently emerged in the literature [30,31]. However, the *in vivo* mechanisms underlying the interrelation between gut microbiota and the above tissues in response to nutritional challenge remain poorly explored.

From the evidence shown in the present paper, it emerges clearly that a fructose-rich diet, known to reshape gut microbiota composition after long term dietary treatment [61,62], impacts gut microbiota also after shorter periods of high sugar intake.

In fact, the analysis of the gut microbial composition revealed a general increase of taxa belonging to the *Lachnospiraceae* family such as *Eubacterium fissicatena, Candidatus Arthromitus, Shuttleworthia*. The *Lachnospiraceae* family is a phylogenetically heterogeneous taxon belonging to the phylum Firmicutes. The role of *Lachnospiraceae* is controversial and their abundance has been often associated with metabolic diseases (*i.e.,* non-alcoholic fatty liver disease [NAFLD], chronic kidney disease, intestinal bowel disease [IBD]), although the taxa of this family are able to produce beneficial metabolites for the host. Indeed, these bacteria are involved in SCFA production, especially butyrate [63]. The increase of the genus *Coprococcus* in fructose-fed rats is in line with our previously published data [61] reporting an increase of *Coprococcus* genus in rats fed a fructose-rich diet for 8 weeks. Bacteria belonging to the *Coprococcus* and *Butyrivibrio* genus are recognized as SCFA producers and contribute to butyrate formation. These findings are in line with the increase of butyrate and propionate concentration that we observed in faecal and plasma samples of fructose-fed animals. Besides the recognized beneficial effects of SCFA, the presence of high amounts of these compounds is not always an indication of a beneficial effect and high SCFA concentrations have also been associated with obesity, hypertension and gut dysbiosis in humans [64].

The fructose-induced increase in bacteria belonging to the *Bacteroides pectinophilus* and *Eubacterium eligens* genera, with putative probiotic potential [65], could be the result of a general dysbio-

Table 1
Summary of metabolic changes.

Parameter	After 3 wk of fructose-rich diet	After 3 wk of switching to control diet
Plasma metabolic parameters		
Glucose during GTT	↑	↑
Insulin during GTT	**ns**	↑
Triglycerides	↑	↑
Skeletal muscle features		
Insulin signaling (pAkt, p-GSK, GLUT-4, insulin sensitivity index)	↓	↓
Glycogen and Proteins	↓	↓
Weight	**ns**	↓
Fructose, Uric Acid, GLUT-5	↑	**ns**
Fatty Acid Synthase,	↑	↑
Triglycerides and ceramide	↓	↑
SK1	↑	↓
SpnS2	**ns**	↓
S1P	↑	**ns**
S1P2	↑	↑
S1P3		
Oxidant-producing enzymes	↑	**ns**
(NADPH oxidase and xanthine	↑	**ns**
oxidase)	↑	**ns**
Oxidative stress markers	↑	↑
(N-Tyrosine and TBARS)	↓	**ns**
Antioxidant enzymes (Catalase, Glutathione reductase)		
Superoxide dismutase		
Mitochondrial enzymes (COX and CS)		
Epididymal WAT features		
Insulin signaling (pAkt, p-GSK, GLUT-4)	↓	**ns**
Weight, weight gain	**ns**	↑
Adipocyte area 250-1500	↓	↓
Adipocyte area >7500,	↑	↑
Adipocyte mean area	↑	**ns**
Fructose, Uric Acid, GLUT-5	↑	**ns**
Fatty Acid Synthase		
Gut microbiota	**altered**	**rescued**
SCFA		
Faecal acetate, propionate, and	↑	**ns**
butyrate	↑	**ns**
Plasma propionate and butyrate	**ns**	**ns**
Plasma acetate		

sis induced by the diet that, by reducing the abundance of other bacteria, could confer a competitive advantage for the proliferation of this genus. Other genera increased with the fructose intake were *Oribacterium* and *Mollicutes* RF39. The genus *Oribacterium* was reported to be closely related to the dysregulation of biliar acids metabolism [66] and obesity [67], while an increase of *Mollicutes* RF39 has been correlated with stress condition in mice [68]. Moreover, a bloom of bacteria belonging to the *Mollicutes* order has been reported as consequence of diet induced obesity in mice [69]. In our analysis we also found a decrease of the genera *Muribaculum* and *Bacillus* in response to a fructose-rich diet. The abundance of these genera is generally associated with healthy status and, in the case of *Muribaculum*, its reduction has been already reported in other pathological conditions such as Chron's disease [70]. Overall our results showed that 3 weeks of high-fructose diet strongly alter the gut microbiota but when this regimen is followed by 3 weeks of standard diet, the intestinal microbiota returns to a composition that resembles that of rats mainained for the entire period under standard diet.

Reshaping of gut microbiota is usually associated with changes in the availability of microbial products, namely SCFA. Our present findings indicate that the fructose-rich diet elicits an increase in the production of acetate, butyrate, and propionate, which are the most abundant SCFA in the gut (constituting >95% of the SCFA content) [71]. The increased faecal concentrations of the three SCFA agree with previous findings showing that higher levels of SCFAs are induced by fructose-rich diet [72–74] and are associated with diet-induced NAFLD and obesity [69,75–78] suggesting possible deleterious effects, perhaps depending on SCFA profile and concentration. In fact, SCFA have also been described to weaken intestinal barrier function and to favor endotoxemia [79]. In addition, increased intestinal IkB-α phosphorylation and permeability have been reported in mice fed an HFD for 8 weeks [80], and downregulation of zonula occludens-1 (ZO-1) has been

reported in conditions associated with increased SCFA and/or high-fructose diets [81]. Interestingly, isotopic tracing of fructose in various mouse models has demonstrated that some carbon sources for the de novo lipogenesis in the liver come from acetate produced by gut microbiota fermentation of fructose [82,83]. In addition, Zhao et al. [83] found a twofold increase in acetate after acute fructose feeding in portal blood but not systemic blood, indicating that acetate is efficiently cleared by the liver. The authors further found that depleting the microbiome markedly blocked fructose conversion into hepatic acetyl-CoA and fatty acids thus concluding that the generation of microbial acetate feeds lipogenic pools of acetyl-CoA in the liver of fructose-fed animals. We have recently found [33] that after 3 weeks of fructose-rich diet the activity of hepatic de novo lipogenic enzymes was significantly upregulated but returned to control levels after switching back to control diet. Therefore, the increased acetate found in fructose-fed rats, once absorbed in the portal vein and delivered to the liver might be metabolized in this tissue for de novo lipid synthesis, thus contributing to the increased hepatic steatosis and plasma triglycerides. This hypothesis is also supported by the finding that acetate concentrations are increased in the faeces but not in the plasma of F rats and that acetate accounts for 80% of the faecal SCFA and 46% of the plasma SCFA.

Our present results also show that switching back to control diet for 3 weeks is however a period long enough to restore the gut bacterial community and consequently the levels of the SCFA. The reversibility of changes in gut microbiota has been investigated with partially discordant results. Some previous papers have reported persistent changes in microbiome composition following changes in the dietary regimen, but the experimental protocol utilized either a longer period (9 weeks) of fructose-rich diet [84], compared to that used in the present study, or a high fat diet [85]. In contrast with the above findings but in agreement with this study, it has been reported that just 1 week is sufficient to restore gut microbiota after 8 weeks of high fat diet [86], or that 2 weeks of control diet partly restore gut microbiota changes elicited by high fat diet [87]. Thus, from our results, it appears that, at least after short periods of enhanced dietary intake of fructose, the modification of gut microbiota is fully reversible.

Since gut microbiota has been involved in the control of energy homeostasis in extra-hepatic tissues, [30,31], we studied skeletal muscle, the major determinant of whole-body glucose homeostasis, and epididymal white adipose tissue, as representative of intraabdominal fat, that is strictly linked to metabolic syndrome, in an attempt to clarify whether the response of these tissues to fructose treatment and sugar removal from the diet reflects the microbiota changes.

Skeletal muscle expresses GLUT5 fructose transporters and has been demonstrated to utilize fructose [88], thus pointing to the possible direct influence of this sugar on skeletal muscle metabolic activity. Our results show an increased content of GLUT5 protein, fructose, as well as of its main metabolic byproduct, uric acid, after 3 weeks of fructose-rich diet. It is well known that fructose metabolism led to ATP depletion, that in the present condition is exacerbated by decreased mitochondrial activity. In addition, uric acid production causes oxidative stress that indeed was found increased after fructose feeding, notwithstanding the compensatory increase in several antioxidant enzymes. This altered metabolic condition was reversed when switching back to control diet.

Notably, whole body glucose tolerance was impaired both after 3 weeks of fructose-rich diet and 3 weeks after switching back to control diet, similarly to what previously found in adult animals [14], and in young rats that exhibited fasting hyperglycemia after 16 d or 6 weeks of fructose intake [89,90].

Therefore, it seems that even brief periods of elevated fructose intake impact on insulin sensitivity, independently from age and importantly, this metabolic impairment is evident well beyond the end of the fructose intake.

Skeletal muscle greatly influences glucose disposal after the first 30 min from ingestion, and we therefore investigated its contribution to the altered glucose tolerance curve, showing that insulin physiological response in this tissue is impaired after fructose intake with this impairment persisting following fructose withdrawal. In fact, three downstream effectors of insulin signaling pathway are less activated in F and FR rats, confirming that insulin delivered to skeletal muscle from the blood does not fully activate its intracellular signaling pathways, thus potentially influencing both glucose and protein metabolism in skeletal muscle. In particular, the decreased inhibition of the enzyme GSK implies inhibition of the pathway of glycogen synthesis and the following decrease in glycogen deposition in this tissue. This detrimental effect can be further worsened by the lower abundance of GLUT4, and hence a slower entry of glucose in the cells. In addition, the reduced effect of insulin on skeletal muscle can also affect its anabolic action and therefore exert an impact on protein metabolism. In agreement, the higher activation of GSK, which is known to inhibit protein synthesis [91], could be the cause of the decreased mass and protein content of hindleg muscles, that does not depend on dietary treatment, since energy intake was the same between control and fructose-fed rats and the two diets contained the same amount of proteins.

Among the cellular factors involved in the development of insulin resistance in skeletal muscle, an important role is played by intramyocellular triglycerides, arising from increased lipid influx or neosynthesis in skeletal muscle [92]. Interestingly, short-term fructose intake elicited an increase in plasma triglycerides that persisted also after fructose withdrawal from the diet. Concomitantly, we here show a persistent increase in the activity of the FAS activity, as well as increased skeletal muscle triglycerides and ceramide, that well correlate with the well-known role of these metabolites in the onset of insulin resistance [93].

Ceramide metabolism is linked to that of S1P, through the action of specific kinases [94], that prevent ceramide accumulation by promoting its conversion into S1P. It has been reported that SK1 is an important enzyme that regulates ceramide metabolism and insulin sensitivity in skeletal muscle, by reducing the accumulation of muscle ceramide in conditions of lipid oversupply. This identifies SK1 as an important regulator of lipid partitioning in skeletal muscle [95]. In agreement, we here report for the first time a significant fructose-induced decrease in SK1 protein levels in skeletal muscle, that could contribute to higher levels of ceramide in this tissue. This finding is intriguing since SK/S1P signalling axis crucially modulates various fundamental processes in skeletal muscle [96], among which the modulation of insulin sensitivity [97]. We also evidenced a fructose-induced increase in the S1P receptors S1P2 and 3 as well as in the specific transporter Spns2. These latter modifications could represent an adaptative response to decreased intracellular synthesis of S1P and stimulate further investigation on the link between sugar-rich diet, insulin sensitivity and sphingosine metabolism. Interestingly, the increased SK1 protein levels evidenced in FR rats may represent a counterregulatory response to increased ceramide levels. However, the increased SK1 levels in FR rats are not mirrored by decreased ceramide content, at least 3 weeks after fructose withdrawal, so we cannot exclude that more time is required to affect skeletal muscle ceramide or that other pathways, such as de novo synthesis, sphingomyelin and glucosylceramide catabolism and ceramide 1-phosphate dephosphorylation, might be involved.

The persistent increase in serum triglycerides can also impact on white adipose tissue physiology. In agreement, following the expansion of eWAT during the whole experimental period, we found changes in the dimensional profile of the adipocytes, with an increase in larger cells at the expense of the smaller ones, together with an expansion of this site of deposition after switching to a control diet. At molecular level, eWAT content of fructose, uric acid and GLUT5, were all upregulated by fructose-rich diet, concomitantly to an increased activity of the lipogenic enzyme FAS, in agreement with findings showing that fructose stimulates de novo fatty acid synthesis in isolated adipocytes [98]. These metabolic changes were coupled with a condition of inflammation that started with the onset of high-fructose diet, persisted also during the rescue period, and was characterized by an increased content of the proinflammatory cytokine TNF-α, an increased activity of the macrophage-linked enzyme myeloperoxidase, increased presence of CLS, and decreased amount of the anti-inflammatory molecule adiponectin. The present findings on the persistence of eWAT hypertrophy even after switching to a control diet agree with recent results showing hypertrophy and inflammation of perigonadal adipocytes in formerly obese mice, with concomitant upregulation of pathways associated with immune function [99]. Coupled with the above modifications, molecular markers of insulin resistance were detected in eWAT, although these latter variations were rescued by switching to control diet. The reversal of insulin resistance in eWAT could be related to the lower lipid pressure on these cells after the interruption of fructose-rich diet, since the flux of lipids into the cells comes only from increased plasma triglycerides, while de novo lipogenesis is switched off.

From the present results it emerges that increased fructose intake even on a short-time basis elicits functional remodeling of metabolically relevant tissues, namely skeletal muscle and adipose tissue, through mechanisms that go well beyond the reshaping of gut microbiota. We previously evidenced that a successful strategy to avoid/limit fructose-induced onset of metabolic syndrome is the modulation of gut microbiota either by antibiotic administration or by faecal transplant [61,62]. Our present results extend this concept by demonstrating that once the reshaping of gut microbiota is elicited, its reversibility is not sufficient to abolish the metabolic alterations triggered in other tissues such as muscle or adipose tissue. Taken together, previous and present results suggest that fructose-induced changes in gut microbiota are involved in the onset of metabolic syndrome but this metabolic imbalance, once started, likely triggers in turn other alterations not directly linked to gut microbiota that persist beyond the changes in dietary treatment.

The persistent elevations of triglycerides and ceramide fit well with persistent insulin resistance exhibited by skeletal muscle. Similarly, in eWAT the persistent flux of plasma triglycerides fuels tissue expansion and inflammation. Therefore, it can be concluded that the persistence of increased plasma triglycerides even after the switching to a control diet following a period of elevated fructose intake, contributes to potentially alter permanently the physiology of metabolically relevant tissues, such as WAT and skeletal muscle (Table 1, Fig. 9). This picture delineates a very harmful situation, considering increasingly consumption of fructose especially in the young populations, that are posed at risk of experiencing stable metabolic modifications that can certainly impact on their health status later in the adulthood.

The findings of this study are of relevance for their transferability to humans, since they emphasize the need for awareness-raising strategies aimed both at a net reduction in the use of added sugars by the food industry, and at a significative decrease in the consumption of sugar-rich food especially during adolescence, to prevent/limit organ alterations in a critical phase of growth till the adult phase. In this sense, a limitation of this study is that, not having followed the animals for a longer time, we cannot say if a fully rescue is possible in the adult age and, if this is the case, how long time is required. A further interesting perspective could be to verify whether strategies based on the administration of dietary supplements (prebiotics, probiotics or antioxidants/anti-inflammatory molecules) could accelerate the full recovery of organ physiology after fructose-rich diets, to promote a healthy growth.

Data availability statement

The data that support the findings of this study are available from the corresponding author upon reasonable request.

Author contributions

AM, SI and LC designed the study. AM, ADP, CG, RC, MN, MS, LB, AA, CF, CD, CB performed the experiments and AM, MS, LB, AA, CD analyzed and graphed the data. SI and LC wrote the paper in consultation with AM, LB and ER. All authors contributed to data interpretation and performed final editing checks and approved the final manuscript.

Funding

This work was supported by a grant from University of Naples Federico II [RD 2021].

Declaration of Competing Interests

The authors declare no conflict of interest.

Acknowledgment

The authors wish to thank Dr. Emilia de Santis for skillful management of animal house.

Supplementary materials

Supplementary material associated with this article can be found, in the online version, at doi:10.1016/j.jnutbio.2022.109247.

References

[1] Dekker MJ, Su Q, Baker C, Rutledge AC, Adeli K. Fructose: a highly lipogenic nutrient implicated in insulin resistance, hepatic steatosis, and metabolic syndrome. Am J Physiol Endocrinol Metab 2010;299:E685–94. doi:10.1152/ajpendo.00283.2010.
[2] Tappy L, Lê KA, Tran C, Paquot N. Fructose and metabolic diseases: new findings, new questions. Nutrition 2010;26:1044–9. doi:10.1016/j.nut.2010.02.014.
[3] Duffey KJ, Huybrechts I, Mouratidou T, Libuda L, Kersting M, De Vriendt T, et al. Beverage consumption among European adolescents in the HELENA study. Eur J Clin Nutr 2012;66(2):244–52. doi:10.1038/ejcn.2011.166.
[4] Defronzo RA, Tripathy D. Skeletal muscle insulin resistance is the primary defect in type 2 diabetes. Diabetes Care 2009;32:S157–63. doi:10.2337/dc09-S302.
[5] Francey C, Cros J, Rosset R, Creze C, Rey V, Stefanoni V, et al. The extra-splanchnic fructose escape after ingestion of a fructose-glucose drink: an exploratory study in healthy humans using a dual fructose isotope method. Clin Nutr ESPEN 2019;29:125–32. doi:10.1016/j.clnesp.2018.11.008.
[6] Douard V, Ferraris RP. Regulation of the fructose transporter GLUT5 in health and disease. Am J Physiol Endocrinol Metab 2008;295:E227–37. doi:10.1152/ajpendo.90245.2008.
[7] Helsley RN, Moreau F, Gupta MK, Radulescu A, DeBosch B. Softic S. Tissue-specific fructose metabolism in obesity and diabetes. Curr Diab Rep 2020;20:1–16. doi:10.1007/s11892-020-01342-8.
[8] Jang C, Hui S, Lu W, Cowan AJ, Morscher RJ, Lee G, et al. The small intestine converts dietary fructose into glucose and organic acids. Cell Metab 2018;27(2):351–61. doi:10.1016/j.cmet.2017.12.016.

[9] Rai AK, Jaiswal N, Maurya CK, Sharma A, Ahmad I, Ahmad S, et al. Fructose-induced AGEs-RAGE signaling in skeletal muscle contributes to impairment of glucose homeostasis. J Nutr Biochem 2019;71:35–44. doi:10.1016/j.jnutbio.2019.05.016.
[10] Rattanavichit Y, Chukijrungroat N, Saengsirisuwan V. Sex differences in the metabolic dysfunction and insulin resistance of skeletal muscle glucose transport following high fructose ingestion. Am J Physiol 2016;311:R1200–12. doi:10.1152/ajpregu.00230.2016.
[11] Baena M, Sangüesa G, Dávalos A, Latasa MJ, Sala-Vila A, Sánchez RM, et al. Fructose, but not glucose, impairs insulin signaling in the three major insulin-sensitive tissues. Sci Rep 2016;6:26149. doi:10.1038/srep26149.
[12] Qin B, Nagasaki M, Ren M, Bajotto G, Oshida Y, Sato Y. Cinnamon extract prevents the insulin resistance induced by a high-fructose diet. Horm Metab Res 2004;36(2):119–25. doi:10.1055/s-2004-814223.
[13] Togashi N, Ura N, Higashiura K, Murakami H, Shimamoto K. The contribution of skeletal muscle tumor necrosis factor-alpha to insulin resistance and hypertension in fructose-fed rats. J Hypertens 2000;18(11):1605–10. doi:10.1097/00004872-200018110-00011.
[14] Crescenzo R, Bianco F, Coppola P, Mazzoli A, Cigliano L, Liverini G, et al. The effect of high-fat–high-fructose diet on skeletal muscle mitochondrial energetics in adult rats. Eur J Nutr 2015;54(2):183–92. doi:10.1007/s00394-014-0699-7.
[15] Crescenzo R, Bianco F, Coppola P, Mazzoli A, Cigliano L, Liverini G, et al. Increased skeletal muscle mitochondrial efficiency in rats with fructose-induced alteration in glucose tolerance. Br J Nutr 2013;110(11):1996–2003. doi:10.1017/S0007114513001566.
[16] Di Meo S, Iossa S, Venditti P. Skeletal muscle insulin resistance: role of mitochondria and other ROS sources. J Endocrinol 2017;233:R15–42. doi:10.1530/JOE-16-0598.
[17] Jaiswal N, Maurya CK, Arha D, Avisetti DR, Prathapan A, Raj PS, et al. Fructose induces mitochondrial dysfunction and triggers apoptosis in skeletal muscle cells by provoking oxidative stress. Apoptosis 2015;20(7):930–47. doi:10.1007/s10495-015-1128-y.
[18] De Stefanis D, Mastrocola R, Nigro D, Costelli P, Aragno M. Effects of chronic sugar consumption on lipid accumulation and autophagy in the skeletal muscle. Eur J Nutr 2017;56(1):363–73. doi:10.1007/s00394-015-1086-8.
[19] Warren BE, Lou PH, Lucchinetti E, Zhang L, Clanachan AS, Affolter A, et al. Early mitochondrial dysfunction in glycolytic muscle, but not oxidative muscle, of the fructose-fed insulin-resistant rat. Am J Physiol Endocrinol Metab 2014;306(6):E658–67. doi:10.1152/ajpendo.00511.2013.
[20] Nyakudya TT, Isaiah S, Ayeleso A, Ndhlala AR, Mukwevho E, Erlwanger KH. Short-term neonatal oral administration of oleanolic acid protects against fructose-induced oxidative stress in the skeletal muscles of suckling Rats. Molecules 2019;24(4):661. doi:10.1016/j.jnutbio.2019.108338.
[21] Marek G, Pannu V, Shanmugham P, Pancione B, Mascia D, Crosson S, et al. Adiponectin resistance and proinflammatory changes in the visceral adipose tissue induced by fructose consumption via ketohexokinase-dependent pathway. Diabetes 2015;64(2):508–18. doi:10.2337/db14-0411.
[22] Crescenzo R, Bianco F, Coppola P, Mazzoli A, Valiante S, Liverini G, et al. Adipose tissue remodeling in rats exhibiting fructose-induced obesity. Eur J Nutr 2014;53(2):413–19. doi:10.1007/s00394-013-0538-2.
[23] Fryklund C, Borg M, Svensson T, Schumacher S, Negoita F, Morén B, et al. Impaired glucose transport in inguinal adipocytes after short-term high-sucrose feeding in mice. J Nutr Biochem 2020;78:108338. doi:10.1016/j.jnutbio.2019.108338.
[24] Qin J, Li Y, Cai Z, Li S, Zhu J, Zhang F, et al. A metagenome-wide association study of gut microbiota in type 2 diabetes. Nature 2012;490(7418):55–60. doi:10.1038/nature11450.
[25] Allin KH, Tremaroli V, Caesar R, Jensen BAH, Damgaard MTF, Bahl MI, et al. Aberrant intestinal microbiota in individuals with prediabetes. Diabetologia 2018;61(4):810–20. doi:10.1007/s00125-018-4550-1.
[26] Albhaisi SAM, Bajaj JS, Sanyal AJ. Role of gut microbiota in liver disease. Am J Physiol Gastrointest Liver Physiol 2020;318(1):G84–98. doi:10.1152/ajpgi.00118.2019.
[27] Allam-Ndoul B, Castonguay-Paradis S, Veilleux A. Gut microbiota and intestinal trans-epithelial permeability. Int J Mol Sci 2020;21(17):6402. doi:10.3390/ijms21176402.
[28] Rooks MG, Garrett WS. Gut microbiota, metabolites and host immunity. Nat Rev Immunol 2016;16(6):341–52. doi:10.1038/nri.2016.42.
[29] Morais LH, Schreiber HL 4th, Mazmanian SK. The gut microbiota-brain axis in behaviour and brain disorders. Nat Rev Microbiol 2021;19(4):241–55. doi:10.1038/s41579-020-00460-0.
[30] Gizard F, Fernandez A, De Vadder F. Interactions between gut microbiota and skeletal muscle. Nutr Metab Insights 2020;13:1178638820980490. doi:10.1177/1178638820980490.
[31] Rodriguez J, Delzenne NM. Modulation of the gut microbiota-adipose tissue-muscle interactions by prebiotics. J Endocrinol 2021;249(1):R1–23. doi:10.1530/JOE-20-0499.
[32] Siersbæk M, Varticovski L, Yang S, Baek S, Nielsen R, Mandrup S, et al. High fat diet-induced changes of mouse hepatic transcription and enhancer activity can be reversed by subsequent weight loss. Sci Rep 2017;7:40220. doi:10.1038/srep40220.
[33] Mazzoli A, Gatto C, Crescenzo R, Cigliano L, Iossa S. Prolonged changes in hepatic mitochondrial activity and insulin sensitivity by high fructose intake in adolescent rats. Nutrients 2021;13(4):1370. doi:10.3390/nu13041370.
[34] Marriott BP, Cole N, Lee E. National estimates of dietary fructose intake increased from 1977 to 2004 in the United States. J Nutr 2009;139(6) 1228S–1235S. doi:10.3945/jn.108.098277.
[35] Abdul-Ghani MA, Matsuda M, Balas B, DeFronzo RA. Muscle and liver insulin resistance indexes derived from the oral glucose tolerance test. Diabetes Care 2007;30(1):89–94. doi:10.2337/dc06-1519.
[36] Roehrig KL, Allred JB. Direct enzymatic procedure for the determination of liver glycogen. Anal Biochem 1974;58(2):414–21. doi:10.1016/0003-2697(74)90210-3.
[37] Crescenzo R, Cigliano L, Mazzoli A, Cancelliere R, Carotenuto R, Tussellino M, et al. Early effects of a low fat, fructose-rich diet on liver metabolism, insulin signaling, and oxidative stress in young and adult rats. Front Physiol 2018;9:411. doi:10.3389/fphys.2018.00411.
[38] Fernandes MA, Custódio JB, Santos MS, Moreno AJ, Vicente JA. Tetrandrine concentrations not affecting oxidative phosphorylation protect rat liver mitochondria from oxidative stress. Mitochondrion 2006;6(4):176–85. doi:10.1016/j.mito.2006.06.002.
[39] Crescenzo R, Spagnuolo MS, Cancelliere R, Iannotta L, Mazzoli A, Gatto C, et al. Effect of initial aging and high-fat/high-fructose diet on mitochondrial bioenergetics and oxidative status in rat brain. Mol Neurobiol 2019;56(11):7651–63. doi:10.1007/s12035-019-1617-z.
[40] Flohé L, Otting F. Superoxide dismutase assays. Methods Enzymol 1984;105:93–104. doi:10.1016/s0076-6879(84)05013-8.
[41] Ac Maehly, Chance B. The assay of catalases and peroxidases. Methods Biochem Anal 1954;1:357–424. doi:10.1002/9780470110171.ch14.
[42] Cos P, Ying L, Calomme M, Hu JP, Cimanga K, Van Poel B, et al. Structure-activity relationship and classification of flavonoids as inhibitors of xanthine oxidase and superoxide scavengers. J Nat Prod 1998;61(1):71–6. doi:10.1021/np970237h.
[43] Bettaieb A, Vazquez Prieto MA, Rodriguez Lanzi C, Miatello RM, Haj FG, Fraga CG, et al. (-)-Epicatechin mitigates high-fructose-associated insulin resistance by modulating redox signaling and endoplasmic reticulum stress. Free Radic Biol Med 2014;72:247–56. doi:10.1016/j.freeradbiomed.2014.04.011.
[44] Barré H, Bailly L, Rouanet JL. Increased oxidative capacity in skeletal muscles from cold-acclimated ducklings: a comparison with rats. Comp Biochem Physiol B 1987;88(2):519–22. doi:10.1016/0305-0491(87)90337-3.
[45] Srere PA. Citrate synthase. Meth Enzymol 1969;13:3–11.
[46] Di Luccia B, Mazzoli A, Cancelliere R, Crescenzo R, Ferrandino I, Monaco A, et al. Lactobacillus gasseri SF1183 protects the intestinal epithelium and prevents colitis symptoms in vivo. J Funct Foods 2018;42:195–202. doi:10.1016/j.jff.2017.12.049.
[47] Cinti S, Mitchell G, Barbatelli G, Murano I, Ceresi E, Faloia E, et al. Adipocyte death defines macrophage localization and function in adipose tissue of obese mice and humans. J Lipid Res 2005;46(11):2347–55. doi:10.1194/jlr.M500294-JLR200.
[48] Chen HC, Smith SJ, Ladha Z, Jensen DR, Ferreira LD, Pulawa LK, et al. Increased insulin and leptin sensitivity in mice lacking acyl CoA:diacylglycerol acyltransferase 1. J Clin Invest 2002;109(8):1049–55. doi:10.1172/JCI14672.
[49] Milani C, Hevia A, Foroni E, Duranti S, Turroni F, Lugli GA, et al. Assessing the fecal microbiota: an optimized ion torrent 16S rRNA gene-based analysis protocol. PLoS One 2013;8(7):e68739. doi:10.1371/journal.pone.0068739.
[50] Caporaso JG, Kuczynski J, Stombaugh J, Bittinger K, Bushman FD, Costello EK, et al. QIIME allows analysis of high-throughput community sequencing data. Nat Methods 2010;7(5):335–6. doi:10.1038/nmeth.f.303.
[51] Callahan BJ, McMurdie PJ, Rosen MJ, Han AW, Johnson AJ, Holmes SP. DADA2: High-resolution sample inference from Illumina amplicon data. Nat Methods 2016;13(7):581–3. doi:10.1038/nmeth.3869.
[52] Bokulich NA, Kaehler BD, Rideout JR, Dillon M, Bolyen E, Knight R, et al. Optimizing taxonomic classification of marker-gene amplicon sequences with QIIME 2's q2-feature-classifier plugin. Microbiome 2018;6(1):90. doi:10.1186/s40168-018-0470-z.
[53] Quast C, Pruesse E, Yilmaz P, Gerken J, Schweer T, Yarza P, et al. The SILVA ribosomal RNA gene database project: improved data processing and web-based tools. Nucleic Acids Res 2013;41(Database issue):D590–6. doi:10.1093/nar/gks1219.
[54] Lozupone C, Knight R. UniFrac: a new phylogenetic method for comparing microbial communities. Appl Environ Microbiol 2005;71(12):8228–35. doi:10.1128/AEM.71.12.8228-8235.2005.
[55] Kaul A, Mandal S, Davidov O, Peddada SD. Analysis of microbiome data in the presence of excess zeros. Front Microbiol 2017;8:2114. doi:10.3389/fmicb.2017.02114.
[56] Cuvillier O, Pirianov G, Kleuser B, Vanek PG, Coso OA, Gutkind S, et al. Suppression of ceramide-mediated programmed cell death by sphingosine-1-phosphate. Nature 1996;381(6585):800–3. doi:10.1038/381800a0.
[57] Blaho VA, Hla T. An update on the biology of sphingosine 1-phosphate receptors. J Lipid Res 2014;55(8):1596–608. doi:10.1194/jlr.R046300.
[58] Chusyd DE, Wang D, Huffman DM, Nagy TR. Relationships between rodent white adipose fat pads and human white adipose fat depots. Front Nutr 2016;3:10. doi:10.3389/fnut.2016.00010.
[59] Gabriely I, Ma XH, Yang XM, Atzmon G, Rajala MW, Berg AH, et al. Removal of visceral fat prevents insulin resistance and glucose intolerance of aging: an adipokine-mediated process? Diabetes 2002;51(10):2951–8. doi:10.2337/diabetes.51.10.2951.
[60] Barzilai N, She L, Liu BQ, Vuguin P, Cohen P, Wang J, Rossetti L. Surgical removal of visceral fat reverses hepatic insulin resistance. Diabetes 1999;48(1):94–8. doi:10.2337/diabetes.48.1.94.

[61] Di Luccia B, Crescenzo R, Mazzoli A, Cigliano L, Venditti P, Walser JC, et al. Rescue of fructose-induced metabolic syndrome by antibiotics or faecal transplantation in a rat model of obesity. PLoS One 2015;10(8):e0134893. doi:10.1371/journal.pone.0134893.
[62] Crescenzo R, Mazzoli A, Di Luccia B, Bianco F, Cancelliere R, Cigliano L, et al. Dietary fructose causes defective insulin signalling and ceramide accumulation in the liver that can be reversed by gut microbiota modulation. Food Nutr Res 2017;61(1):1331657. doi:10.1080/16546628.2017.1331657.
[63] Vacca M, Celano G, Calabrese FM, Portincasa P, Gobbetti M, De Angelis M. The controversial role of human gut Lachnospiraceae. Microorganisms 2020;8(4):573. doi:10.3390/microorganisms8040573.
[64] de la Cuesta-Zuluaga J, Mueller NT, Álvarez-Quintero R, Velásquez-Mejía EP, Sierra JA, Corrales-Agudelo V, et al. Higher fecal short-chain fatty acid levels are associated with gut microbiome dysbiosis, obesity, hypertension and cardiometabolic disease risk factors. Nutrients 2018;11(1):51. doi:10.3390/nu11010051.
[65] Brahe LK, Le Chatelier E, Prifti E, Pons N, Kennedy S, Hansen T, et al. Specific gut microbiota features and metabolic markers in postmenopausal women with obesity. Nutr Diabetes 2015;5(6):e159. doi:10.1038/nutd.2015.9.
[66] Petrov PD, Garcia-Mediavilla MV, Guzman C, Porras D, Nistal E, Martinez-Florez S, et al. A network involving gut microbiota, virculating bile acids, and hepatic metabolism genes that protects against non-alcoholic fatty Llver disease. Mol Nutr Food Res 2019;63:e1900487. doi:10.1002/mnfr.201900487.
[67] Angelakis E, Armougom F, Carriere F, Bachar D, Laugier R, Lagier JC, et al. A metagenomic investigation of the duodenal microbiota reveals links with obesity. PLoS ONE 2015;10:e0137784. doi:10.1371/journal.pone.0137784.
[68] Usui N, Matsuzaki H, Shimada S. Characterization of early life stress-affected gut microbiota. Brain Sci 2021;11:913. doi:10.3390/brainsci11070913.
[69] Turnbaugh PJ, Bäckhed F, Fulton L, Gordon JI. Diet-induced obesity is linked to marked but reversible alterations in the mouse distal gut microbiome. Cell Host Microbe 2008;3(4):213–23. doi:10.1016/j.chom.2008.02.015.
[70] Dobranowski PA, Tang C, Sauvé JP, Menzies SC, Sly LM. Compositional changes to the ileal microbiome precede the onset of spontaneous ileitis in SHIP deficient mice. Gut Microbes 2019;10(5):578–98. doi:10.1080/19490976.2018.1560767.
[71] Canfora EE, Jocken JW, Blaak EE. Short-chain fatty acids in control of body weight and insulin sensitivity. Nat Rev Endocrinol 2015;11(10):577–91. doi:10.1038/nrendo.
[72] Bhat SF, Pinney SE, Kennedy KM, McCourt CR, Mundy MA, Surette MG, et al. Exposure to high fructose corn syrup during adolescence in the mouse alters hepatic metabolism and the microbiome in a sex-specific manner. J Physiol 2021;599(5):1487–511. doi:10.1113/JP280034.
[73] Rivero-Gutiérrez B, Gámez-Belmonte R, Suárez MD, Lavín JL, Aransay AM, Olivares M, et al. A synbiotic composed of Lactobacillus fermentum CECT5716 and FOS prevents the development of fatty acid liver and glycemic alterations in rats fed a high fructose diet associated with changes in the microbiota. Mol Nutr Food Res 2017;61(8). doi:10.1002/mnfr.201600622.
[74] Brütting C, Lara Bisch M, Brandsch C, Hirche F, Stangl GI. Impact of dietary propionate on fructose-induced changes in lipid metabolism, gut microbiota and short-chain fatty acids in mice. Int J Food Sci Nutr 2021;72(2):160–73. doi:10.1080/09637486.2020.1773415.
[75] Schwiertz A, Taras D, Schäfer K, Beijer S, Bos NA, Donus C, et al. Microbiota and SCFA in lean and overweight healthy subjects. Obesity (Silver Spring) 2010;18(1):190–5. doi:10.1038/oby.2009.167.
[76] Fernandes J, Su W, Rahat-Rozenbloom S, Wolever TM, Comelli EM. Adiposity, gut microbiota and faecal short chain fatty acids are linked in adult humans. Nutr Diabetes 2014;4(6):e121. doi:10.1038/nutd.2014.23.
[77] Rahat-Rozenbloom S, Fernandes J, Gloor GB, Wolever TM. Evidence for greater production of colonic short-chain fatty acids in overweight than lean humans. Int J Obes (Lond) 2014;38(12):1525–31. doi:10.1038/ijo.2014.46.
[78] Turnbaugh PJ, Ley RE, Mahowald MA, Magrini V, Mardis ER, Gordon JI. An obesity-associated gut microbiome with increased capacity for energy harvest. Nature 2006;444(7122):1027–31. doi:10.1038/nature05414.
[79] Sánchez de Medina F, Romero-Calvo I, Mascaraque C, Martínez-Augustin O. Intestinal inflammation and mucosal barrier function. Inflamm Bowel Dis 2014;20(12):2394–404. doi:10.1097/MIB.0000000000000204.
[80] Ritze Y, Bárdos G, Claus A, Ehrmann V, Bergheim I, Schwiertz A, et al. Lactobacillus rhamnosus GG protects against non-alcoholic fatty liver disease in mice. PLoS One 2014;9(1):e80169. doi:10.1371/journal.pone.0080169.
[81] Miele L, Valenza V, La Torre G, Montalto M, Cammarota G, Ricci R, et al. Increased intestinal permeability and tight junction alterations in nonalcoholic fatty liver disease. Hepatology 2009;49(6):1877–87. doi:10.1002/hep.22848.
[82] Raman M, Ahmed I, Gillevet PM, Probert CS, Ratcliffe NM, Smith S, et al. Fecal microbiome and volatile organic compound metabolome in obese humans with nonalcoholic fatty liver disease. Clin Gastroenterol Hepatol 2013;11(7):868–75. doi:10.1016/j.cgh.2013.02.015.
[83] Zhao S, Jang C, Liu J, Uehara K, Gilbert M, Izzo L, et al. Dietary fructose feeds hepatic lipogenesis via microbiota-derived acetate. Nature 2020;579(7800):586–91. doi:10.1038/s41586-020-2101-7.
[84] Kim H, Worsley O, Yang E, Purbojati RW, Liang AL, Tan W, et al. Persistent changes in liver methylation and microbiome composition following reversal of diet-induced non-alcoholic-fatty liver disease. Cell Mol Life Sci 2019;76(21):4341–54. doi:10.1007/s00018-019-03114-4.
[85] Thaiss CA, Itav S, Rothschild D, Meijer MT, Levy M, Moresi C, et al. Persistent microbiome alterations modulate the rate of post-dieting weight regain. Nature 2016 22;540(7634):544–51. doi:10.1038/nature20796.
[86] Safari Z, Monnoye M, Abuja PM, Mariadassou M, Kashofer K, Gérard P, et al. Steatosis and gut microbiota dysbiosis induced by high-fat diet are reversed by 1-week chow diet administration. Nutr Res 2019;71:72–88. doi:10.1016/j.nutres.2019.09.004.
[87] Shang Y, Khafipour E, Derakhshani H, Sarna LK, Woo CW, Siow YL, et al. Short term high fat diet induces obesity-enhancing changes in mouse gut microbiota that are partially reversed by cessation of the high fat diet. Lipid 2017;52(6):499–511. doi:10.1007/s11745-017-4253-2.
[88] Darakhshan F, Hajduch E, Kristiansen S, Richter EA, Hundal HS. Biochemical and functional characterization of the GLUT5 fructose transporter in rat skeletal muscle. Biochem J 1998;336(Pt 2):361–6. doi:10.1042/bj3360361.
[89] Dupas J, Goanvec C, Feray A, Guernec A, Alain C, Guerrero F, et al. Progressive induction of type 2 diabetes: effects of a reality– like fructose enriched diet in young Wistar rats. PLoS ONE 2016;11(1):e0146821. doi:10.1371/journal.pone.0146821.
[90] Li KP, Yuan M, He ZR, Wu Q, Zhang CM, Lei ZL, et al. Omics insights into metabolic stress and resilience of rats in response to short-term fructose overfeeding. Mol Nutr Food Res 2019;63(23):e1900773. doi:10.1002/mnfr.201900773.
[91] Vyas DR, Spangenburg EE, Abraha TW, Childs TE, Booth FW. GSK-3beta negatively regulates skeletal myotube hypertrophy. Am J Physiol Cell Physiol 2002;283(2):C545–51. doi:10.1152/ajpcell.00049.2002.
[92] Amati F, Dubé JJ, Alvarez-Carnero E, Edreira MM, Chomentowski P, Coen PM, et al. Skeletal muscle triglycerides, diacylglycerols, and ceramides in insulin resistance: another paradox in endurance-trained athletes? Diabetes 2011;60(10):2588–97. doi:10.2337/db10-1221.
[93] Metcalfe LK, Smith GC, Turner N. Defining lipid mediators of insulin resistance - controversies and challenges. J Mol Endocrinol 2018. doi:10.1530/JME-18-0023.
[94] Donati C, Cencetti F, Bruni P. Sphingosine 1-phosphate axis: a new leader actor in skeletal muscle biology. Front Physiol 2013;4:338. doi:10.3389/fphys.2013.00338.
[95] Bruce CR, Risis S, Babb JR, Yang C, Kowalski GM, Selathurai A, et al. Overexpression of sphingosine kinase 1 prevents ceramide accumulation and ameliorates muscle insulin resistance in high-fat diet-fed mice. Diabetes 2012;61(12):3148–55. doi:10.2337/db12-0029.
[96] Bruni P, Donati C. Pleiotropic effects of sphingolipids in skeletal muscle. Cell Mol Life Sci 2008;65(23):3725–36. doi:10.1007/s00018-008-8236-6.
[97] Rapizzi E, Taddei ML, Fiaschi T, Donati C, Bruni P, Chiarugi P. Sphingosine 1-phosphate increases glucose uptake through trans-activation of insulin receptor. Cell Mol Life Sci 2009;66(19):3207–18. doi:10.1007/s00018-009-0106-3.
[98] Varma V, Boros LG, Nolen GT, Chang CW, Wabitsch M, Beger RD, et al. Metabolic fate of fructose in human adipocytes: a targeted 13C tracer fate association study. Metabolomics 2015;11(3):529–44. doi:10.1007/s11306-014-0716-0.
[99] Fischer IP, Irmler M, Meyer CW, Sachs SJ, Neff F, Hrabě de Angelis M, et al. A history of obesity leaves an inflammatory fingerprint in liver and adipose tissue. Int J Obes (Lond) 2018;42(3):507–17. doi:10.1038/ijo.2017.224.